

# Molecular composition and volatility of multi-generation products formed from isoprene oxidation by nitrate radical

Rongrong Wu<sup>1,2</sup>, Luc Vereecken<sup>1</sup>, Epameinondas Tsiligiannis<sup>3</sup>, Sungah Kang<sup>1</sup>, Sascha R. Albrecht<sup>1,a</sup>, Luisa Hantschke<sup>1</sup>, Defeng Zhao<sup>4</sup>, Anna Novelli<sup>1</sup>, Hendrik Fuchs<sup>1</sup>, Ralf Tillmann<sup>1</sup>, Thorsten Hohaus<sup>1</sup>, Philip T.M. Carlsson<sup>1</sup>, Justin Shenolikar<sup>5</sup>, François Bernard<sup>6</sup>, John N. Crowley<sup>5</sup>, Juliane L. Fry<sup>7</sup>, Bellamy Brownwood<sup>7</sup>, Joel A. Thornton<sup>8</sup>, Steven S. Brown<sup>9,10</sup>, Astrid Kiendler-Scharr<sup>1</sup>, Andreas Wahner<sup>1</sup>, Matthias Hallquist<sup>3</sup>, Thomas F. Mentel<sup>1\*</sup>

<sup>1</sup>Institute of Energy and Climate Research, Troposphere (IEK-8), Forschungszentrum Jülich GmbH, 52428 Jülich, Germany

<sup>2</sup>College of Environmental Sciences and Engineering, State Key Joint Laboratory of Environmental Simulation and Pollution Control, Peking University, 100871, Beijing, China

<sup>3</sup>Department of Chemistry and Molecular Biology, University of Gothenburg, 41296, Gothenburg, Sweden

<sup>4</sup>Department of Atmospheric and Oceanic Sciences & Institute of Atmospheric Sciences, Fudan University, 200438, Shanghai, China

<sup>5</sup>Atmospheric Chemistry Department, Max Planck Institut für Chemie, 55128 Mainz, Germany

<sup>6</sup>Institut de Combustion, Aérothermique, Réactivité et Environnement (ICARE), UPR CNRS, 45071 Orléans, France

<sup>7</sup>Department of Chemistry, Reed College, Portland, OR 97202, USA

<sup>8</sup>Department of Atmospheric Sciences, University of Washington, Seattle, WA 98195, USA

<sup>9</sup>NOAA Chemical Sciences Laboratory, Boulder, CO 80305, USA

<sup>10</sup>Department of Chemistry, University of Colorado, Boulder, CO 80309, USA

<sup>a</sup>present address: SOLIDpower GmbH, 52525 Heinsberg, Germany

\*Correspondence to: Thomas F. Mentel (t.mentel@fz-juelich.de)

## Abstract

Isoprene oxidation by nitrate radical ( $\text{NO}_3$ ) is a potentially important source of secondary organic aerosol (SOA). It is suggested that the second or later-generation products are the more substantial contributors to SOA. However, there are few studies investigating the multi-generation chemistry of isoprene- $\text{NO}_3$  reaction, and information about the volatility of different isoprene nitrates, which is essential to evaluate their potential to form SOA and determine their atmospheric fate, is rare. In this work, we studied the reaction between isoprene and  $\text{NO}_3$  in the SAPHIR chamber (Jülich) under near atmospheric conditions. Various oxidation products were measured by a high-resolution time-of-flight chemical ionization mass spectrometer using  $\text{Br}^-$  as the reagent ion. **Most of the products detected are organic nitrates, and they are grouped into monomers ( $\text{C}_4$ - and  $\text{C}_5$ -products), and dimers ( $\text{C}_{10}$ -products) with 1–3 nitrate groups according to their chemical composition.** Most of the observed products match expected termination products observed in previous studies, but some compounds such as monomers and dimers with three nitrogen atoms were rarely reported in the literature as gas-phase products from isoprene oxidation by  $\text{NO}_3$ . Possible formation mechanisms for these compounds are proposed. The multi-generation chemistry of isoprene and  $\text{NO}_3$  is characterized by taking advantages of the time behavior of different products. In addition, the vapor pressures of diverse isoprene nitrates are calculated by different parametrization methods. An estimation of the vapor pressure is also derived from their condensation behavior. According to our results, isoprene monomers belong to intermediate volatility or semi-volatile organic compounds and thus have little effect on SOA formation. In contrast, the dimers are expected to have low or

43 extremely low volatility, indicating that they are potentially substantial contributors to SOA. However, the  
44 monomers constitute 80% of the total explained signals on average, while the dimers contribute less than 2%,  
45 suggesting that the contribution of isoprene NO<sub>3</sub> oxidation to SOA by condensation should be low under  
46 atmospheric conditions. We expect a SOA mass yield of about 5 % from the wall loss and dilution corrected  
47 mass concentrations, assuming that all of the isoprene dimers in the low- or extremely low-volatility organic  
48 compound (LVOC or ELVOC) range will condense completely.

## 49 1. Introduction

50 Atmospheric submicron aerosols have an adverse effect on air quality, human health and climate (Jimenez et al.,  
51 2009; Pöschl, 2005). Secondary organic aerosol (SOA), which is formed from oxidation of volatile organic  
52 compounds (VOC) followed by gas-to-particle partitioning, comprise a large fraction (20-90%) of the  
53 submicron aerosol mass (Jimenez et al., 2009; Zhang et al., 2007). It is confirmed that a significant proportion of  
54 SOA arises from biogenic VOC (BVOC) oxidation (Hallquist et al., 2009; Spracklen et al., 2011).

55 Isoprene is globally the most abundant non-methane volatile organic compound originating from  
56 vegetation, with emissions estimated to be 440-660 Tg yr<sup>-1</sup> (Guenther et al., 2012). Due to its high abundance, as  
57 well as its high reactivity with atmospheric oxidants, isoprene plays a significant role in tropospheric chemistry,  
58 and its chemistry affects the global aerosol burden and distribution (Carlton et al., 2009; Fry et al., 2018; Ng et  
59 al., 2008, 2017; Surratt et al., 2010), although its SOA yield is much lower than those of monoterpenes and  
60 sesquiterpenes (Friedman and Farmer, 2018; Kim et al., 2015; Marais et al., 2016; , McFiggans, et al. 2019;  
61 Mutzel et al., 2016; Ng et al., 2007, 2008; Surratt et al., 2010; Thornton et al., 2020). Recent model simulations  
62 suggested the isoprene-derived SOA production is 56.7 Tg C yr<sup>-1</sup>, contributing up to 41% of global SOA  
63 (Stadtler et al., 2018). Observations in southeastern United States suggested that isoprene-derived SOA makes  
64 up 17- 48% of total organic aerosol (Hu et al., 2015; Kim et al., 2015; Marais et al., 2016). As a consequence, it  
65 is essential to fully characterize the potential of isoprene to form condensable products and its contribution to  
66 SOA formation (Carlton et al., 2009).

67 Although the majority of isoprene emissions is emitted by plants and is light-dependent, isoprene emitted  
68 in the day can persist in the boundary layer after sunset, and its mixing ratio can remain as high as several ppb  
69 (Brown et al., 2009; Starn et al., 1998; Stroud et al., 2002; Warneke et al., 2004). Generally During the daytime,  
70 isoprene is primarily oxidized by the hydroxyl radical (OH) and somewhat by ozone (O<sub>3</sub>), in the daytime but its  
71 main oxidizers shift to nitrate radical (NO<sub>3</sub>) and O<sub>3</sub> in the nighttime (Wennberg et al., 2018). Due to the higher  
72 reactivity of NO<sub>3</sub> with isoprene At night when the concentration of OH is negligible, the nitrate radical (NO<sub>3</sub>)  
73 and O<sub>3</sub> become the predominant oxidants of isoprene. Reaction of isoprene with NO<sub>3</sub> is competitive to that with  
74 O<sub>3</sub> because of its much larger rate constant ( $k_{NO_3} = 6.5 \times 10^{-13} \text{ cm}^3 \text{ molecules}^{-1} \text{ s}^{-1}$  and  $k_{O_3} = 1.28 \times 10^{-17} \text{ cm}^3$   
75 molecules<sup>-1</sup>s<sup>-1</sup> at 298 K, respectively, IUPAC), a considerable fraction of the residual isoprene would be  
76 oxidized by NO<sub>3</sub> at night, even if the mixing ratio of NO<sub>3</sub> is 10,000 time lower than that of O<sub>3</sub> and therefore  
77 nocturnal nitrate radical chemistry is typically thought to be of significant importance for isoprene, especially in  
78 regions where sufficient nitrogen oxides are available (Brown et al., 2009; Fry et al., 2018; Ng et al., 2017;  
79 Wennberg et al., 2018). Although reaction with NO<sub>3</sub> only represents ~ 5-6% of isoprene loss, it accounts for a  
80 large proportion of ~~isoprene nitrates~~ organic nitrates derived from isoprene oxidation (~ 40-50%) (Wennberg et  
81 al., 2018). Therefore, reaction of isoprene with NO<sub>3</sub> is a potential source of SOA. In addition, it is found from  
82 both laboratory and chamber experiments that the SOA yield of isoprene from NO<sub>3</sub> oxidation is higher than that  
83 from OH or O<sub>3</sub> oxidation, which is typically less than 5% (Carlton et al., 2009; Dommen et al., 2009;  
84 Kleindienst et al., 2007; Kroll et al., 2006). For example, Ng et al. (2008) concluded the isoprene SOA yield  
85 from NO<sub>3</sub> was in the range of 4.3% to 23.8%, depending on RO<sub>2</sub> fate (higher SOA yield when the experiments  
86 were dominated by RO<sub>2</sub>+RO<sub>2</sub> rather than RO<sub>2</sub>+NO<sub>3</sub> reaction). Rollins et al. (2009) also observed a high SOA  
87 yield from isoprene (14%) when both of its double bonds were oxidized by NO<sub>3</sub>. In an aircraft study in the  
88 southeastern United States, Fry et al. (2018) derived an isoprene-NO<sub>3</sub> SOA yield as large as 27% on average

89 under high NO<sub>x</sub> conditions, although their mass yield estimation was indirect, and based on a molar yield  
90 determination of 9 ± 5%. In light of the relatively high SOA yield from NO<sub>3</sub> oxidation, even though only a  
91 minor fraction of isoprene is oxidized by NO<sub>3</sub>, the SOA formed at nighttime would still probably be comparable  
92 to that produced at daytime (Brown et al., 2009; Fry et al., 2018).

93 However, isoprene-NO<sub>3</sub> chemistry ([Wennberg et al. 2018](#), [Vereecken et al. 2021](#)) has received less  
94 attention than the extensively studied OH- or O<sub>3</sub>-initiated oxidation (Barber et al., 2018; Novelli et al., 2020;  
95 Peeters et al., 2014; Wang et al., 2018; Wennberg et al., 2018; Whalley et al., 2012). It has been recognized that  
96 later-generation oxidation of isoprene by NO<sub>3</sub> makes more significant contribution to SOA formation (Carlton et  
97 al., 2009; Fry et al., 2018; Rollins et al., 2009). Nevertheless, although the importance of multi-generation NO<sub>3</sub>  
98 oxidation of isoprene to SOA formation has been recognized, few studies extended the investigation beyond the  
99 first-generation oxidation, and details of isoprene-NO<sub>3</sub> multi-generation chemistry are still lacking.

100 Organic compounds, especially highly oxygenated organic molecules (HOM) that have low or extremely  
101 low volatility, contribute significantly to SOA formation by condensation, or even form new particles (Bianchi  
102 et al., 2019; Ehn et al., 2014; Kirkby et al., 2016, Tröstl et al., 2016). Previous studies have confirmed that low-  
103 volatility products from isoprene-NO<sub>3</sub> reaction are the major precursors to SOA (Ng et al., 2008; Rollins et al.,  
104 2009; Schwantes et al., 2019). Here the low-volatility compounds refer to gas phase products that allow  
105 fractions to exist in particle-phase, and may include the groups of organic compounds with intermediate  
106 volatility (IVOC, 300 < C\* < 3 × 10<sup>6</sup> μg m<sup>-3</sup>), semi-volatility (SVOC, 0.3 < C\* < 300 μg m<sup>-3</sup>), low volatility (LVOC,  
107 3 × 10<sup>-5</sup> < C\* < 0.3 μg m<sup>-3</sup>) and extremely low volatility (ELVOC, C\* < 3 × 10<sup>-5</sup> μg m<sup>-3</sup>) as proposed by Donahue et al.  
108 (2012). In general, SVOC, LVOC and ELVOC can contribute to the SOA formation (Jimenez et al., 2009). In  
109 order to evaluate the potential of oxygenated products to form SOA, information about their vapor pressures is  
110 essential. However, due to the high degree of functionalization, low or extremely low volatility, as well as  
111 uncertainties in quantification and molecular structures, it is challenging to determine the exact vapor pressure  
112 of highly oxidized products. Detailed information on the volatilities of different generation products is lacking,  
113 which impedes the assessment of their contribution to SOA formation.

114 In this work, we present the results of chamber experiments on isoprene oxidation by NO<sub>3</sub> under near  
115 atmospheric conditions, where NO<sub>3</sub> was produced in situ by O<sub>3</sub> reaction with NO<sub>2</sub>. Subsequent characteristics of  
116 multi-generation chemistry of isoprene with NO<sub>3</sub> are investigated. By examining the time evolution of various  
117 gas-phase products, we propose possible reaction mechanisms that help to get the possible functionalization of  
118 the products. Saturation vapor pressures of the major gas-phase products observed by HR-ToF-CIMS are  
119 predicted by using different parameterization methods that are widely-used or state-of-the-art in literature. In  
120 addition, we estimate the vapor pressure derived from equilibrium partitioning coefficient according to the  
121 condensation behavior of different products in experiments with and without seed aerosols. Based on these  
122 results, the volatility of the major oxidation products stemming from isoprene-NO<sub>3</sub> reaction and their potential  
123 to form SOA are evaluated.

## 124 2. Experimental and methods

### 125 2.1 Atmospheric simulation chamber SAPHIR

126 All the data presented here were measured in the atmospheric simulation chamber SAPHIR (Simulation of  
127 Atmospheric PHotochemical In a large Reaction Chamber) at Forschungszentrum Jülich, Germany, which is  
128 designed to investigate the oxidation processes of both biogenic and anthropogenic trace gases and formation of  
129 secondary particles and pollutants under near atmospheric conditions. The SAPHIR chamber is a double-walled  
130 Teflon (FEP) cylinder with a volume of 270 m<sup>3</sup> (5 meters in diameter and 18 meters in length). The large  
131 volume-to-surface ratio (1 m) allows experiments to be conducted under natural conditions and reduces  
132 interference from the chamber walls. The chamber is equipped with a shutter system which can be opened to  
133 admit sunlight for photochemical experiments or closed to mimic nighttime conditions. There are two fans  
134 inside the chamber to ensure good mixing of trace gases (within 2 minutes). The chamber is filled with synthetic  
135 air made from mixing of ultrapure nitrogen and oxygen (Linde, purity  $\geq 99.99990\%$ ) and is slightly over-  
136 pressured ( $\sim 35$  Pa) to prevent intrusion of outside air into the chamber. Due to small leakage ( $\sim 7$  m<sup>3</sup> h<sup>-1</sup>) and  
137 gas consumption by instrument sampling, a replenishment flow is provided by a flow control, which leads to a  
138 dilution rate of 4%–7% per hour. A more detailed description of the chamber set-up and its characterization can  
139 be found elsewhere (Rohrer et al., 2005).

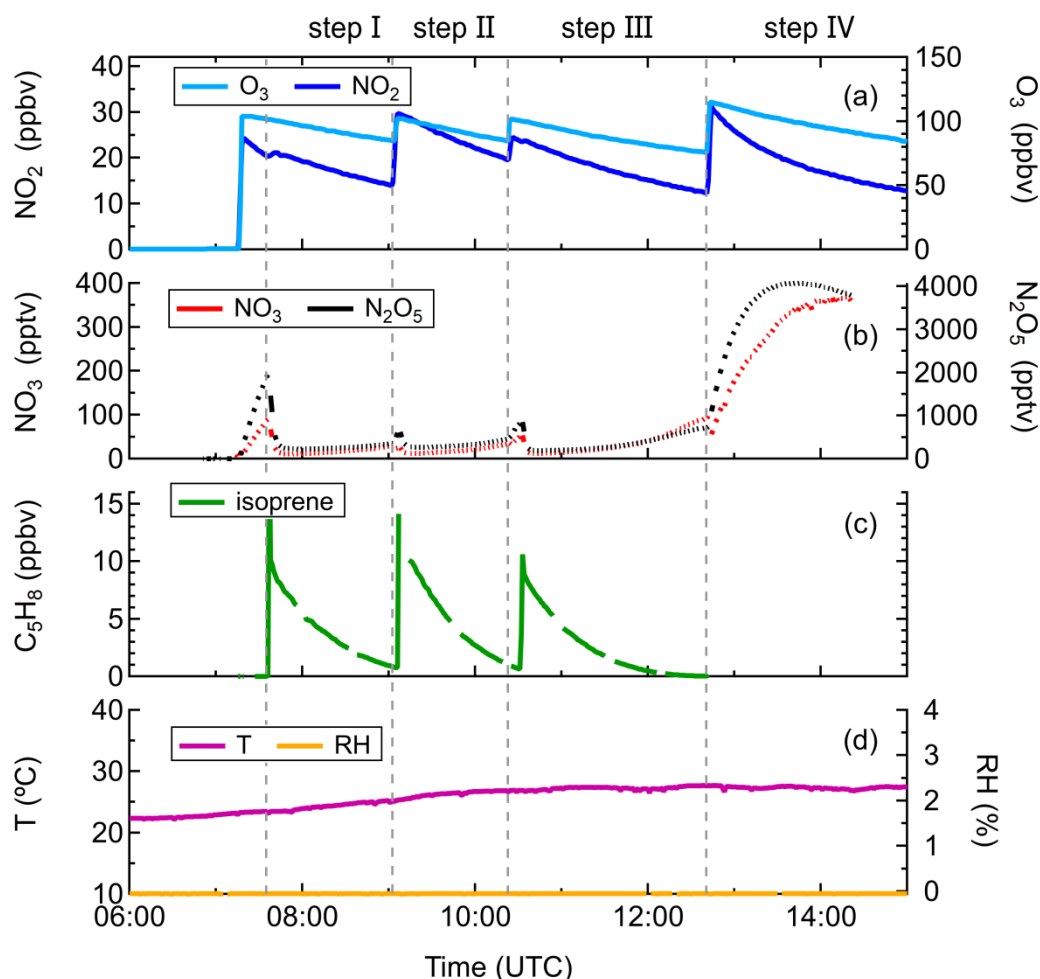
### 140 2.2 Experiment description

141 A series of experiments investigating the oxidation of isoprene by NO<sub>3</sub> were conducted in the SAPHIR chamber  
142 in August 2018 (ISOPNO<sub>3</sub> campaign) under different chemical conditions. In this work, we primarily focus on  
143 an experiment conducted on 08 August 2018 that examined the fast oxidation of isoprene by NO<sub>3</sub> (up to  $\sim 130$   
144 pptv) without seed aerosols. The experiment was performed under dry (RH < 5%) and dark condition, and  
145 employed injections of O<sub>3</sub> and NO<sub>2</sub> as source of NO<sub>3</sub>, where O<sub>3</sub> was generated by a silent discharge ozoniser  
146 (O3onia), and high-purity NO<sub>2</sub> was introduced from a gas bottle (Linde, purity >99%).

147 Before the experiment, the chamber was flushed overnight with a total amount of  $\sim 1800$  m<sup>3</sup> synthetic air to  
148 minimize any remaining contamination. At the beginning of the experiment, the chamber air was slightly  
149 humidified (RH < 0.1%) by flushing water vapor from boiling Milli-Q<sup>®</sup> water into the chamber. Thereafter, O<sub>3</sub>  
150 and NO<sub>2</sub> were added to the chamber in succession, and their concentrations in the chamber after injection were  
151 approximately 100 and 25 ppbv, respectively, as shown in Fig. 1. After that,  $\sim 10$  ppbv of isoprene was injected  
152 using a GC syringe, initiating the reaction with NO<sub>3</sub>. The period between the first and second injection is  
153 defined as “step I”, as so on for the other three periods. ~~The second injection was done when After almost~~  
154 ~~complete consumption of isoprene from the first injection was almost completely consumed, to reach~~  
155 ~~concentrations of another 100, 30, and 10 ppbv of O<sub>3</sub>, NO<sub>2</sub>, and isoprene in the chamber of ~100, 30, and 10~~  
156 ~~ppbv, respectively, were added. After another About 1.5 hours later, the chemistry was further accelerated~~  
157 ~~again by the a third injection of precursors, and accordingly the concentrations of O<sub>3</sub>, NO<sub>2</sub>, and isoprene reached~~  
158 ~~~ 100, 25, and 10 ppbv, respectively, after the injection.~~ Two hours later, the fourth addition was made and the  
159 concentrations of O<sub>3</sub> and NO<sub>2</sub> increased to approximately 115 ppbv and 30 ppbv, respectively, aiming to  
160 promote further oxidation of early generation products. In total the system was kept running for about 7.5 h.  
161 ~~According to the modeling results Calculation from measurements of isoprene, O<sub>3</sub>, OH, NO<sub>3</sub> and dilution,~~  
162 ~~indicates that NO<sub>3</sub> contributed for more than approximately 90% of the chemical losses of isoprene reacted with~~

163 ~~NO<sub>3</sub>, as shown in Fig. S1, indicating that reaction with~~ reaction with O<sub>3</sub> was being a minor sink of  
 164 ~~isoprene pathway~~ in our system. The reaction of isoprene with OH was not considered as OH concentration was  
 165 below the detection limit of the instrument in this study (Fig. S2). Thus, losses due to reaction with OH could  
 166 not be quantified from the measurement, but have been determined to contribute about 10% of the isoprene  
 167 losses according to a recently published modelling work based on the same campaign, with the contribution of  
 168 the NO<sub>3</sub> reaction accounting for up to 80% accordingly (Vereecken et al., 2021).

169 A complementary experiment was conducted on 14 August 2018 under similar conditions but with seed  
 170 aerosols. Approximately 60 μg m<sup>-3</sup> of ammonium sulfate aerosol was added at the beginning of the experiment.  
 171 Thereafter, approximate 100 and 20 ppbv of O<sub>3</sub> and NO<sub>2</sub> were introduced to the chamber to produce NO<sub>3</sub>,  
 172 followed by addition of ~10 ppbv of isoprene in about 30 minutes later (see Fig. S4S3). Another 6 ppbv of NO<sub>2</sub>  
 173 and 10 ppbv of isoprene were added about one hour later to accelerate the reaction. At the last injection, only O<sub>3</sub>  
 174 (~ 50 ppbv) and NO<sub>2</sub> (~ 7 ppbv) were added, similar as for the experiment without seeds. The experiment lasted  
 175 for about 8 h. The results were used to investigate the condensation behavior of various gas-phase products from  
 176 isoprene oxidation, aiming to estimate equilibrium partitioning coefficients and vapor pressures.



177  
 178 **Figure 1: Measurements of (A) O<sub>3</sub> and NO<sub>2</sub>, (B) NO<sub>3</sub> and N<sub>2</sub>O<sub>5</sub>, (C) isoprene and (D) temperature and relative**  
 179 **humidity in the chamber during the experiment on 08 August, 2018.**

## 180 2.3 Instrumentation

181 A high-resolution time-of-flight chemical ionization mass spectrometer (HR-ToF-CIMS, Aerodyne Research  
182 Inc., hereafter CIMS) was used to continuously measure the gas-phase products from isoprene oxidation by NO<sub>3</sub>.  
183 The ToF-MS was operated in ‘V’ mode with the mass resolution power between 3000–4000 Th/Th. In order to  
184 reduce the losses of HO<sub>2</sub> radicals and HOM on the tubing, a customized inlet (Albrecht et al., 2019) was directly  
185 connected to the chamber. The CIMS was operated in negative ion mode using Br<sup>-</sup> as the reagent ion, which is  
186 selective to polar species such as acids, hydroxy or nitrooxy carbonyls, as well as HO<sub>2</sub> radicals (Albrecht et al.,  
187 2019; Ng et al., 2008; Rissanen et al., 2019; Riva et al., 2019).

188 Bromide ions were generated by passing a mixture of 10 standard cubic centimeters per minute of 0.4%  
189 CF<sub>3</sub>Br in nitrogen and 2 standard liter per minute nitrogen through a 370 MBq <sup>210</sup>Po source (Type P-2021-5000,  
190 NDR Static Control LLC, USA), resulting in ~10<sup>5</sup> ion counts per second (Albrecht et al., 2019). In our system,  
191 ~~on average, about 190 ions were identified for each mass spectrum on average, most of which were detected as~~  
192 ~~adducts with Br<sup>-</sup>, while some acidic compounds (~ 7% of the total) like nitric acid (HNO<sub>3</sub>), glycolic acid~~  
193 ~~(C<sub>2</sub>H<sub>4</sub>O<sub>3</sub>), and malonic acid (C<sub>3</sub>H<sub>4</sub>O<sub>4</sub>) were also detected as deprotonated ions. In addition, there were some ions~~  
194 ~~(~ 10% of the total) identified as adducts with NO<sub>3</sub><sup>-</sup>; most compounds were detected as adducts with Br<sup>-</sup>, but~~  
195 ~~some strong acidic compounds like nitric acid were also detected as deprotonated ions.~~ The isotope distribution  
196 of <sup>79</sup>Br and <sup>81</sup>Br is approximately 1:1, therefore two signals appear at  $m/z = MW+79$  and  $m/z = MW+81$  with  
197 MW being the molecular mass of the molecule that is detected as cluster with Br<sup>-</sup>. In this work, we will use  
198 Thomson (Th) as the unit for mass-to-charge ( $m/z$ ), and the  $m/z$  of molecules discussed in following include the  
199 mass contribution from Br<sup>-</sup> ( $m/z$  79) if there is no other annotation.

200 In order to have an indicator of the CIMS performance, perfluoropentanoic acid (PFPA, C<sub>5</sub>F<sub>9</sub>HO<sub>2</sub>) was  
201 used as an internal standard. ~~For  $m/z$  calibration, five isolated peaks were used, including Br<sup>-</sup> ( $m/z$  79), H<sub>2</sub>OBr<sup>-</sup>~~  
202 ~~( $m/z$  97), HNO<sub>3</sub>Br<sup>-</sup> ( $m/z$  142), C<sub>5</sub>F<sub>9</sub>O<sub>2</sub><sup>-</sup> ( $m/z$  263), and C<sub>5</sub>F<sub>9</sub>HO<sub>2</sub>Br<sup>-</sup> ( $m/z$  343), covering the mass range of~~  
203 ~~dominant products. The averaged accuracies of all five calibrated masses were below 5 ppm over the whole~~  
204 ~~measurement period. However, due to the low signal intensity, the PFPA cluster (C<sub>10</sub>F<sub>18</sub>O<sub>4</sub>H<sup>-</sup>,  $m/z$  527) was not~~  
205 ~~suited for mass calibration, and there were no other suitable masses with sufficient intensity and high accuracy~~  
206 ~~that could be used to calibrate the higher mass range. Therefore, peak fitting in the mass range between 300 to~~  
207 ~~500+ Th might have higher uncertainties.~~ The CIMS was optimized to gain a maximum signal of [HO<sub>2</sub>\*Br]<sup>-</sup>  
208 isotopes, which are weakly bounded clusters. This was achieved by adjusting step by step the electrostatic field  
209 in the transfer stage to minimize fragmentation. During the campaign, the settings of CIMS were kept  
210 unchanged to keep a similar performance. However, the signal of reagent ion Br<sup>-</sup> decreased by about 65% (from  
211 ~ 100, 000 to 34, 000 counts s<sup>-1</sup>) over the campaign duration of four weeks. In order to minimize the effect of  
212 drift in performance, we used the normalized (by the sum of the total ion counts) signals for analysis. The  
213 sensitivity for total carbon was calculated by determining the slope of wall-loss corrected total carbon signals  
214 detected by CIMS (only the identified peaks were considered) versus isoprene consumed. As illustrated in Fig.  
215 ~~S2aS4a~~, the CIMS sensitivities were roughly identical in two experiments (0.026 ± 0.002 norm. count s<sup>-1</sup> ppbv<sup>-1</sup>  
216 on 08 August, and 0.022 ± 0.001 norm. count s<sup>-1</sup> ppbv<sup>-1</sup> on 14 August), indicating that different experimental  
217 conditions over two days had an insignificant impact on CIMS sensitivity for total carbon and thus the data from  
218 these days are comparable. In addition, an inter-comparison of measurements by Br<sup>-</sup> CIMS and I<sup>-</sup> CIMS were  
219 made. As shown in Fig. ~~S2bS4b~~, the measurements of C<sub>5</sub>H<sub>6</sub>N<sub>2</sub>O<sub>8</sub> from the two instruments are well linearly

220 correlated with each other at the early oxidation stages. However, ~~the correlation coefficient somewhat changes~~  
221 ~~between the two experiments, which is possibly related to the interference from isomers and the differences in~~  
222 ~~sensitivity between the two instruments~~ the correlation coefficients of measurements from two instruments  
223 ~~deviated from experiment to experiment. This is probably related to different experimental conditions, which~~  
224 ~~might lead to different chemical processes and thus formation of isomers. Since CIMS with different reagent~~  
225 ~~ions might have different sensitivities to isomers, and may be selective for different compounds, the correlation~~  
226 ~~coefficients of measurements from Br<sup>-</sup> and I<sup>-</sup> CIMS may differ from day to day. Moreover, the Br<sup>-</sup> CIMS was~~  
227 ~~not tuned during the campaign while the I<sup>-</sup> CIMS was optimized from time to time.~~ In general, the performance  
228 of Br<sup>-</sup> CIMS was stable and the data taken by it are reliable.

229 The mass spectra data were processed using the software “Tofware” embedded in Igor as provided by  
230 Aerodyne Research Inc. (<https://www.tofwerk.com/software/tofware/?cn-reloaded=1>). Peaks detected in the  
231 mass spectra could be isolated and identified according to their exact mass, and molecular formulas and the  
232 corresponding intensities were obtained by high-resolution peak fitting. Due to a lack of authentic standards for  
233 the products, it is difficult to quantitatively determine their individual absolute concentrations, but we have  
234 calculated the bulk sensitivity for organonitrates by ~~determining the slope of total~~ using the sum of organic  
235 nitrate signals ~~detected by~~ from Br<sup>-</sup> CIMS divided by measurements of the total alkyl nitrates from a thermal  
236 dissociation-cavity ring-down spectrometer during the experiment versus the alkyl nitrate concentrations  
237 measured by a thermal dissociation-cavity ring down spectrometer, as shown in Fig. S2e. The estimated bulk  
238 sensitivities for organonitrates are  $0.016 \pm 0.001$  and  $0.022 \pm 0.001$  norm. count s<sup>-1</sup> ppbv<sup>-1</sup> on 08 August and 14  
239 August, respectively, as shown in Fig. S4c, comparable to the sensitivity for total carbon, but smaller than the  
240 sensitivity for salicylic acid determined by an independent calibration ( $163$  norm. count  $\mu\text{g}^{-1}$  on average as  
241 shown in Fig. S2dS4d, equal to  $0.07$  norm. count s<sup>-1</sup> ppbv<sup>-1</sup>). The bulk sensitivity for organonitrates enables  
242 estimation of the absolute concentrations of products assuming that they have identical sensitivity. In this study  
243 we use the normalized signals instead of absolute concentrations for analysis. This is sufficient here because our  
244 analysis focuses on the time evolution of signals and the relative changes of intensities, so the absolute  
245 concentrations are not necessarily needed. The sensitivity derived above is only used to convert the signals of  
246 dimers to concentrations in order to estimate the SOA yield.

247 Isoprene was measured by a Vocus proton transfer reaction time-of-flight mass spectrometer (Aerodyne  
248 Research Inc., hereafter Vocus), which has a higher mass resolving power (nominal 10000 Th/Th) and less inlet  
249 wall losses and sampling delays compared to traditional PTR-MS (Krechmer et al., 2018). The mixing ratio of  
250 O<sub>3</sub> was monitored by an UV absorption instrument, and that of NO<sub>2</sub> was monitored by a chemiluminescence  
251 instrument and a custom-built cavity ring-down spectrometer (CRDS). The concentrations of NO<sub>3</sub> and N<sub>2</sub>O<sub>5</sub>  
252 were detected by two custom-built CRDS instruments (Dubé et al., 2006; Sobanski et al., 2016). In addition,  
253 temperature and pressure inside the chamber were monitored by an ultra-sonic anemometer and a pressure  
254 sensor, respectively. The relative humidity was primarily detected as water mixing ratio by a Picarro CRDS  
255 instrument (Crosson, 2008).

256 The particle number concentrations and their size distributions were measured by a condensation particle  
257 counter (TSI 3783, hereafter CPC) and a scan mobility particle sizer (TSI 3081 electrostatic classifier combined  
258 with TSI 3025 CPC, hereafter SMPS). The aerosol chemical composition was identified by a high-resolution  
259 time of flight aerosol mass spectrometer (HR-ToF-AMS, Aerodyne Research Inc., hereafter AMS). The



260 ionization efficiency of AMS was determined by using the monodisperse aerosol generated from  $\text{NH}_4\text{NO}_3$  and  
261  $(\text{NH}_4)_2\text{SO}_4$  solutions. The collection efficiency (CE) could be estimated based on the particle mass concentration  
262 yielded from AMS and that derived from SMPS. In this study, the average CE value of 0.5 is used for correction.

## 263 2.4 Methods to estimate saturation vapor pressure

264 The pure liquid saturation vapor pressure is a thermodynamic metric relevant for the partitioning equilibrium of  
265 organic molecules, which determines their propensity to form SOA (Compernelle et al., 2011; O'Meara et al.,  
266 2014; Pankow and Asher, 2008). Due to their complex functionalities and low or extremely low volatility, it is  
267 challenging to determine the vapor pressures of highly oxidized molecules. As a result, theoretical and  
268 semiempirical methods are usually used for vapor pressure estimation. Commonly used semiempirical methods  
269 include composition-activity (CA), group-contribution (GC), and structure-activity (SA) methods. The CA  
270 methods are the easiest to use, as they only require information on molecular composition for estimation. They  
271 are widely applied in context of the two-dimensional volatility basis set (2D-VBS) (Donahue et al., 2011). For  
272 GC methods, the exact functional groups are required to calculate the saturation vapor pressure. The SIMPOL.1  
273 (Pankow and Asher, 2008), the parameterization as described by Nannoolal et al. (2008), and EVAPORATION  
274 (Compernelle et al., 2011) are three widely used GC methods. Structure-activity methods can provide more  
275 accurate estimates with sophisticated treatments of intramolecular interactions like intramolecular hydrogen-  
276 bonding (Bilde et al., 2015). However, detailed molecular properties such as boiling point and evaporation  
277 enthalpy are required for estimation, which are generally obtained by complex and time-consuming quantum  
278 chemical calculations. Therefore, SA methods are not applied for vapor pressure estimation in this study.

279 Saturation concentration ( $C^*$ , mass based) is related to saturation vapor pressure and can be calculated  
280 following Eq. (1) (Donahue et al., 2006). The  $\log_{10}(C^*)$  is a metric used in the 2D-VBS method to evaluate the  
281 volatility of organic molecules.

$$282 C_i^* = \frac{M_i 10^6 \zeta_i p_i^\circ}{RT} \quad (1)$$

283 where  $R$  ( $8.206 \times 10^{-5} \text{ m}^3 \text{ atm K}^{-1} \text{ mol}^{-1}$ ) is the gas constant,  $T$  (K) is the temperature,  $M_i$  ( $\text{g mol}^{-1}$ ) is the molecular  
284 weight of compound  $i$ ,  $\zeta_i$  is the activity coefficient of compound  $i$  and here is assumed to be 1 (Donahue et al.,  
285 2006),  $p_i^\circ$  (atm) is the pure liquid saturation vapor pressure at temperature  $T$  (298 K).

286 In this study, different CA methods are applied to calculate the saturation vapor pressures of various  
287 oxidation products from isoprene reaction with  $\text{NO}_3$ . These include parameterizations that were constrained by  
288 chamber measurements as proposed by Donahue et al. (2011), Mohr et al. (2019), and Peräkylä et al. (2019). All  
289 of these three parameterization methods have included the effect of the presence of nitrate groups on vapor-  
290 pressure estimation. Further we test the GC methods proposed by Nannoolal et al. (2008), Pankow and Asher  
291 (2008, SIMPOL.1), and Compernelle et al. (2011, EVAPORATION). All the methods used in this study are  
292 summarized in Table 1. The calculations of EVAPORATION and the Nannool method were done via the online  
293 molecular and multiphase property prediction facility UManSysProp  
294 ([http://umansysprop.seaes.manchester.ac.uk/tool/vapour\\_pressure](http://umansysprop.seaes.manchester.ac.uk/tool/vapour_pressure)). For the latter the boiling point  
295 parameterization method needs to be predefined, and that from Nannoolal et al. (2004) was adopted as  
296 recommended by O'Meara et al. (2014). The information about molecular structures needed for the calculation  
297 is inferred from mechanistic information, which is described in detail in Sect. 2.5.

**Table 1: Summary of estimation methods of saturation vapor pressure used in this study**

Estimation method	Methodology	Input information			Reference
		molecular formula	functional groups	others	
Donahue et al.	CA <sup>a</sup>	√			Donahue et al., 2011
Mohr et al.	<u>ICA</u> <sup>b</sup>	√			Mohr et al., 2019
Peräkylä et al.	<u>ICA</u> <sup>b</sup>	√			Peräkylä et al., 2020
Nannoolal et al.	<del>GC</del> <sup>b</sup> <u>GC</u> <sup>c</sup>	√	√	√ <sup>d</sup>	Nannoolal et al., 2008
SIMPOL.1	GC	√	√		Pankow and Asher, 2008
EVAPORATION	GC	√	√		Compernelle et al., 2011
This study	<u>EXP</u> <sup>e</sup> <u>EXP</u> <sup>e</sup>				

299 <sup>a</sup> abbreviation of composition-activity method; <sup>b</sup> abbreviation of improved composition-activity method, which  
300 modified the parameterization based on chamber measurements to better fit HOMs; <sup>b,c</sup> abbreviation of group-  
301 contribution method; ~~<sup>c</sup> abbreviation of experimental method~~; <sup>d</sup> boiling point parameterization method is also  
302 required to be defined; <sup>e</sup> abbreviation of experimental method.

303 In addition, we take advantage of the measurements in this study to calculate the gas-particle equilibrium  
304 partitioning coefficient (K) by comparing experiments with and without seed aerosols. The partitioning  
305 coefficient K can be converted to saturation concentration C\* by Eq. (2).

$$306 \quad K_i = \frac{C_{i,p}}{C_{i,g} \times C_{OA}} = \frac{1}{C_i^*} \quad (2)$$

307 where  $C_{i,g}$  and  $C_{i,p}$  are the gas- and particle-phase concentrations ( $\mu\text{g m}^{-3}$ ) of species  $i$ , respectively, and  $C_{OA}$  is  
308 the organic aerosol concentration ( $\mu\text{g m}^{-3}$ ). In this study,  $C_{i,g}$  is signal of species  $i$  from CIMS in the experiment  
309 with seeds, and  $C_{i,p}$  is the difference of signals between experiment without and with seeds (under the same  
310 isoprene consumption condition). The  $C_{OA}$  in the experiment with seeds is in a range of 1-4  $\mu\text{g m}^{-3}$ .

## 311 2.5 Pathways to the multifunctional oxidation products

### 312 2.5.1 Basic peroxy and alkoxy radical chemistry

313 As mentioned before, information about molecular structures (at least functional groups) is required to calculate  
314 vapor pressures by using GC methods. Although the high-resolution ToF-CIMS allows for determining  
315 chemical composition of the detected ions, it is unable to provide information about molecular structures, so that  
316 the constitutional or configurational isomers with the same mass cannot be distinguished without additional  
317 information. Fortunately, knowledge of detailed chemical formation mechanisms can help inferring the  
318 molecular structure information. However, the development of a comprehensive, multi-generational kinetic  
319 mechanism for NO<sub>3</sub>-initiated oxidation of isoprene is outside the scope of the current paper. Instead, in order to  
320 link the observed mass peaks to representative molecular structures, we developed a framework tracing the  
321 chemical oxidation mechanisms by taking well-known oxidation steps to predict the most likely isomeric forms  
322 of the functionalized products formed in the isoprene oxidation. For this purpose, we rely on the extensive

323 literature on isoprene, alkylperoxy radical, and alkoxy radical chemistry (Atkinson, 2007; Atkinson and Arey,  
 324 2003; Bianchi et al., 2019; Crouse et al., 2013; Ehn et al., 2014; Jenkin et al., 2015; [Jenkin et al., 2019](#); Kwan  
 325 et al., 2012; Mentel et al., 2015; Ng et al., 2008; [Noveli et al., 2021](#); Orlando et al., 2003; Orlando and Tyndall,  
 326 2012; Rollins et al., 2009; Schwantes et al., 2015; Vereecken and Francisco, 2012; Vereecken and Peeters,  
 327 [2009, 2010](#); [Vereecken et al., 2021](#); Wennberg et al., 2018; [Ziemann and Atkinson, 2012](#)). This framework is  
 328 depicted in the supporting information and will be discussed in more detail in Sect. 2.5.2 and Sect. 2.5.3. They  
 329 are based on the following main reactivity trends.

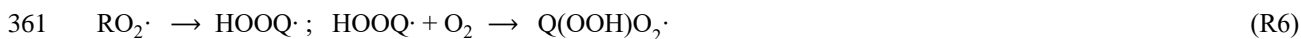
330 Generally, RO<sub>2</sub> radicals can react with other RO<sub>2</sub> and HO<sub>2</sub> radicals. There are three major channels for the  
 331 reaction between two RO<sub>2</sub> radicals, leading to alkoxy radicals (RO) (Reaction R1a), as well as termination  
 332 products like alcohols, aldehydes or ketones (Reaction R1b) and accretion products (Reaction R1c). These  
 333 reactions should take place with the first-generation peroxy radicals, as well as with the higher generation RO<sub>2</sub>  
 334 radicals formed in the later oxidation steps. Hydroperoxides can be formed from the reaction of RO<sub>2</sub> with HO<sub>2</sub>  
 335 radicals (Reaction R2a). This reaction can also yield alkoxy radicals (Reaction R2b).



341 In the presence of NO<sub>x</sub>, RO<sub>2</sub> radicals can also react with NO and NO<sub>2</sub>, leading to the formation of alkoxy  
 342 radicals (R3a), organic nitrates (R3b), and peroxy nitrates (R4) (including peroxyacyl nitrates, PANs, if R =  
 343 R'C(O)-). The channel that results in RO radicals is the major pathway for the reaction of RO<sub>2</sub> radicals with NO  
 344 (Ziemann and Atkinson, 2012). However, reactions of RO<sub>2</sub> radicals with NO (Reaction R3a and R3b) can be  
 345 neglected in this study due to the high O<sub>3</sub> concentration, which results in rapid conversion of NO to NO<sub>2</sub>. The  
 346 peroxy nitrates formed from the reaction of RO<sub>2</sub> with NO<sub>2</sub> will undergo rapid thermal decomposition under our  
 347 experimental conditions, with exception of PANs. The reaction of RO<sub>2</sub> with NO<sub>3</sub> radicals mainly forms NO<sub>2</sub> and  
 348 alkoxy radicals (Reaction R5), which will continue the radical chains (Reaction R7).



353 In addition to bimolecular reactions, intramolecular rearrangement (H-migration) is a competitive reaction  
 354 pathway for RO<sub>2</sub> radicals. RO<sub>2</sub> radicals can undergo H-migration to form a hydroperoxy functionality (-OOH)  
 355 and a radical site that can subsequently recombine with an O<sub>2</sub> molecule, leading to the formation of a new, more  
 356 oxidized substituted RO<sub>2</sub> (Reaction R6). This process is the so-called "autoxidation" path and has been  
 357 confirmed as a significantly important way for SOA formation (Crouse et al., 2013; Ehn et al., 2014; Mentel et  
 358 al., 2015; Praske et al., 2018; Rissanen et al., 2014). The rates of RO<sub>2</sub> H-migration are strongly dependent on the  
 359 structure of RO<sub>2</sub> radicals, and the most likely routes can be derived based on the structure-activity relationship  
 360 proposed by Vereecken and Nozière (2020).



362 The RO radicals formed in the reaction of  $\text{RO}_2 + \text{RO}_2$  typically have three accessible pathways,  
 363 including isomerization by H-migration (Reaction R7a), fragmentation (Reaction R7b) and less important here,  
 364 reaction with  $\text{O}_2$  (Reaction R7c). Like H-migration in  $\text{RO}_2$ , rearrangement by H-shift in RO radicals leads to the  
 365 formation of more oxidized  $\text{RO}_2$  radicals. Fragmentation leads to smaller carbon chains, and this becomes more  
 366 important for alkoxy radicals with a higher number of (oxygen-bearing) substituents (Vereecken and Peeters,  
 367 2009, 2010).



371 In addition to the above general reaction pathways, we include a number of other reactions in the  
 372 framework, such as fragmentation of peroxy radicals, epoxidation of  $\beta$ -OOH alkyl radicals, and unimolecular  
 373 termination of nitrooxy or hydroperoxyl peroxy radicals. Details can be found in the supporting information.

### 374 2.5.2 Formation of first-generation products

375 Here “first-generation products” refers to the closed-shell compounds from the first attack of  $\text{NO}_3$  at the  
 376 isoprene double bonds, while “second-generation products” follow an addition of  $\text{NO}_3$  to the remaining double  
 377 bond (or any other oxidation reaction) of a first-generation product. Addition of a  $\text{NO}_3$  radical to one of isoprene  
 378 double bonds and subsequent addition of  $\text{O}_2$  to the resulting (delocalized) radical sites leads to the formation of  
 379 nitrooxy alkylperoxy radicals ( $\text{INO}_2$ ,  $\text{C}_5\text{H}_8\text{NO}_3$ ). Since isoprene contains two double bonds,  $\text{NO}_3$  can attack any  
 380 of the four positions on the conjugated carbon bonds, resulting in eight possible  $\text{INO}_2$  isomers (including six  
 381 constitutional and two conformational isomers), as shown in Scheme S1. However, both theoretical and  
 382 experimental studies suggest that the addition occurs preferably at the primary and terminal carbons, wherein C1  
 383 addition seems to be preferred over C4 addition (Schwantes et al., 2015; Suh et al., 2001; Wennberg et al., 2018).  
 384 As the GC methods have limited or no ability to distinguish between positional isomers (Kurten et al., 2016), we  
 385 take exemplarily the products following the C1 addition for the vapor pressure analysis in this study.

386 The initial peroxy radicals ( $\text{C}_5\text{H}_8\text{NO}_3$ ) can undergo rearrangement by H shift from C–H bonds with  
 387 subsequent  $\text{O}_2$  addition, yielding new –OOH functionalized peroxy radicals (Reaction R6). Repeating this  
 388 process can lead to the formation of a series of peroxy radicals and termination products with stepwise  
 389 increasing number of oxygen atoms by 2, as shown in the conceptual scheme Scheme S2. This is the  $\text{RO}_2$   
 390 autoxidation channel and the molecular formula of peroxy radicals formed via consecutive  $\text{O}_2$  additions can be  
 391 represented as  $\text{C}_5\text{H}_8\text{NO}_{(3+2n)}$  ( $n \geq 1$ , number of autoxidation steps). The autoxidation chain can be terminated  
 392 when the H-shift occurs at a carbon with an –OOH or – $\text{ONO}_2$  group attached, leading to carbonyl formation  
 393 with OH or  $\text{NO}_2$  loss (Anglada et al., 2016; Bianchi et al., 2019; Vereecken, 2008; Vereecken et al., 2004). The  
 394 closed-shell products formed in these termination steps have the general molecular formula  $\text{C}_5\text{H}_7\text{NO}_{(5+2n-1)}$  (OH  
 395 loss channel) or  $\text{C}_5\text{H}_8\text{O}_{(3+2n-2)}$  ( $\text{NO}_2$  loss channel).

396 The  $\text{C}_5\text{H}_8\text{NO}_{(3+2n)}$  peroxy radicals can also react with  $\text{HO}_2$  radicals to form –OOH functionalized  
 397 termination products with the general molecular formula  $\text{C}_5\text{H}_9\text{NO}_{(3+2n)}$  (Reaction R2a), or yielding the alkoxy  
 398 radicals  $\text{C}_5\text{H}_8\text{NO}_{(3+2n-1)}$  (Reaction R2b). In addition, the  $\text{C}_5\text{H}_8\text{NO}_{(3+2n)}$  peroxy radicals can react with other  $\text{RO}_2$

399 radicals (Reaction R1a-R1c). The reaction R1a leads to the formation of alkoxy radicals ( $C_5H_8NO_{(3+2n-1)}$ ) while  
400 R1b forms closed-shell products either with a carbonyl group ( $C_5H_7NO_{(3+2n-1)}$ ) or a hydroxyl group  
401 ( $C_5H_9NO_{(5+2n-1)}$ ). Alternatively, dimers can be formed following Reaction R1c, which have then two  $-ONO_2$   
402 groups and at least 8 oxygen atoms depending on the formula of  $RO_2$  radicals involved, as shown in Table S1.

403 The alkoxy radicals from reactions R1a and R2b can undergo unimolecular rearrangement by H shift with  
404 subsequent  $O_2$  addition, similar to the  $RO_2$  radicals, forming new  $RO_2$  radicals with a  $-OH$  group (Reaction  
405 R7a). As mentioned above, when the H-shift occurs at a carbon with an  $-OOH$  or  $-ONO_2$  group attached, the  
406 resulting intermediates tend to lose an OH group or  $NO_2$  (Bianchi et al., 2019), yielding the closed-shell  
407 carbonyl products with general formulas  $C_5H_7NO_{(5+2n-2)}$  or  $C_5H_8O_{(3+2n-3)}$  respectively, as shown in the conceptual  
408 scheme Scheme S3. The newly-formed  $RO_2$  radicals from alkoxy H-shift channel can follow the peroxy  
409 pathways (Reaction R1-R6) like other  $RO_2$  radicals, leading to a diversity of compounds like hydroperoxides  
410 (Reaction R2a,  $C_5H_9NO_{(3+2n+1)}$ ), alcohols (Reaction R1b,  $C_5H_9NO_{(3+2n)}$ ), aldehydes (Reaction R1b,  $C_5H_7NO_{(3+2n)}$ )  
411 as well as accretion products (Reaction R1c,  $C_{10}H_{16}N_2O_x$ ), as depicted in Scheme S3. Alternatively, they can  
412 also yield alkoxy radicals again following reactions R1a and R2b and continue so on. Furthermore, the alkoxy  
413 radicals can break apart into two fragments according to Reaction R7b.

414 In general, the alkoxy reaction pathways diversify the parity of the oxygen number of the products from the  
415 reaction of isoprene with  $NO_3$ , and the compounds formed via these reactions generally have one less or one  
416 more oxygen atom compared to those formed from straight peroxy reaction pathways. With help of the  
417 mechanistic framework described above, we can infer the functionality of first-generation products. This is  
418 exemplified in Scheme S5 and S6 for the major first-generation  $C_5$  products. In addition, the reaction pathways  
419 and their corresponding structures of the first-generation  $C_{10}$  dimers ( $C_{10}H_{16}N_2O_x$ ) are summarized in Scheme  
420 S13.

### 421 2.5.3 Formation of second-generation products

422 Nitrate radicals can oxidize the first-generation products once again at the double bond remaining ( $k_{NO_3}(298K) \sim$   
423  $3-11 \times 10^{14} \text{ cm}^3 \text{ molecule}^{-1} \text{ s}^{-1}$ , Wennberg et al., 2018). This leads eventually to “second-generation” products that  
424 contain at least two nitrogen atoms. Addition of  $NO_3$  radical to the remaining double bond of the first-generation  
425 products results in the formation of dinitrooxy peroxy radicals. We assume that dinitrooxy peroxy radicals can  
426 undergo unimolecular and bimolecular reactions (Reaction R1–R6) in analogy to nitrooxy peroxy radicals,  
427 which lead to secondary products containing two or more nitrogen atoms, as summarized in the conceptual  
428 scheme Scheme S4.

429 The reaction of first-generation nitrooxy peroxy radicals with  $NO_2$  can also yield 2N-compounds (Reaction  
430 R4), however these 2N-compounds ought to be under first-generation products by definition. Such species are  
431 not discussed in detail here but will be covered to catch the diversity of the functionalities for the vapor pressure  
432 estimation. With the help of this secondary reaction framework, we can propose functional groups for the major  
433 second-generation products. Scheme S8 – S10 depict the detailed (possible) reaction pathways that lead to the  
434 formation of detected  $C_5$  dinitrates, as well as their possible structures. Furthermore, the proposed formation  
435 mechanism and their structures for  $C_5$  trinitrates are shown in Scheme S12, while those for the second-  
436 generation  $C_{10}$  dimers ( $C_{10}H_{17}N_3O_x$  and  $C_{10}H_{18}N_4O_x$ ) are depicted in Scheme S13.

## 437 2.5.4 Formation of fragmentation products

438 In addition to the multigenerational C<sub>5</sub> and C<sub>10</sub> products, fragmentation products can be formed from the  
439 reaction of isoprene with NO<sub>3</sub>. As mentioned above, the alkoxy radicals can undergo C–C bond scission,  
440 producing a carbonyl compound and an alkyl fragment (Reaction R7b). As shown in Scheme S7, when the  
441 secondary nitrooxy alkoxy radicals from the further oxidation of C<sub>5</sub> carbonyl compounds (C<sub>5</sub>H<sub>8</sub>O<sub>2</sub> and C<sub>5</sub>H<sub>8</sub>O<sub>3</sub>  
442 here) undergo unimolecular decomposition, C<sub>4</sub> carbonyl products (C<sub>4</sub>H<sub>7</sub>NO<sub>5</sub> and C<sub>4</sub>H<sub>7</sub>NO<sub>6</sub>, respectively) are  
443 formed as well as formyl radicals. Since the bond fission can occur at different positions, the generation of more  
444 reactive C<sub>2</sub> and C<sub>3</sub> carbonyl compounds are possible. In addition, the C<sub>4</sub> carbonyl compounds are possibly  
445 generated through peroxy radical arrangement by 1,4 H-shift and subsequent acyl radical bond scission reactions  
446 (see Scheme S7). The C<sub>4</sub> dinitrates can be formed following similar chemistry, as depicted in Scheme S11.

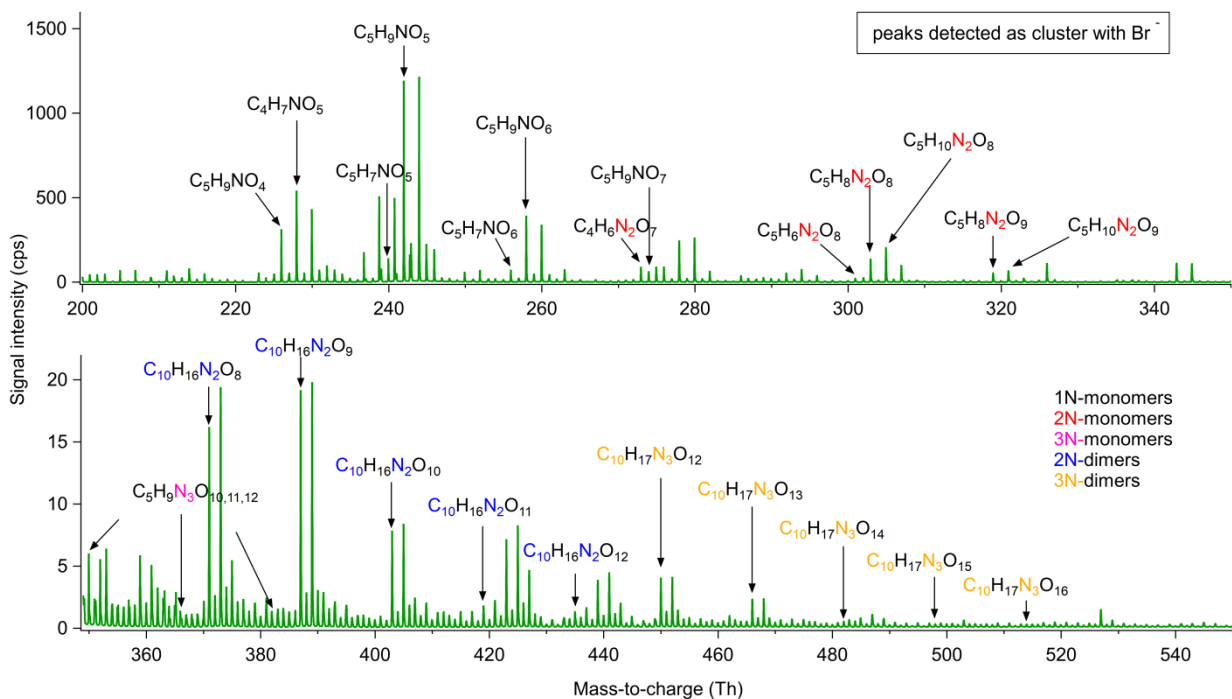
## 447 2.5.5 Candidate structures for vapor pressure estimation

448 Among all gas-phase products detected by CIMS, we selected 32 major representative organonitrates formed  
449 from isoprene oxidation by NO<sub>3</sub> radicals. Their structures are rationalized by the corresponding molecular  
450 formulas and proposed formation mechanisms in the reaction framework. Table S2 summarizes all the  
451 exemplified structures used for vapor pressure estimation. The functional groups covered in the selected  
452 structures include nitrate, hydroxyl, ketone, aldehyde, carboxylic acid, peroxide, hydroperoxide, hydroperoxy  
453 acid, peroxyxynitrate, peroxyacyl nitrate and epoxide. The structural information allows calculation of the  
454 saturation vapor pressure by GC methods.

## 455 3. Results and discussion

### 456 3.1 Chemical composition of oxidation products

457 Figure 2 illustrates the average mass spectra of the whole experiment measured by BrCIMS for isoprene-NO<sub>3</sub>  
458 reaction. Chemical sum formulas were attributed to most of the detected ions. The gas-phase products were  
459 separated into two major groups according to their chemical composition, including monomers comprising C<sub>5</sub>  
460 compounds and dimers containing C<sub>10</sub> compounds. There were also products from decomposition reactions with  
461 C<sub><5</sub>, which were merged into monomers. The monomers and dimers were further classified into five subgroups  
462 as follows. Monomers consisting of compounds with one nitrogen atom (hereafter 1N-monomers) and two or  
463 three N atoms (2N- or 3N-monomers) mainly accumulate in *m/z* 220–280 Th, *m/z* 300–340 Th and 350–390 Th,  
464 respectively, while dimers containing compounds with two N atoms (2N-dimers) and three N atoms (3N-dimers)  
465 appear in *m/z* 370–440 Th and 450–520 Th, respectively. As shown in Fig. 2, the signal intensities decrease  
466 from 1N-monomers, 2N-monomers, 2N-dimers to 3N-monomers and 3N-dimers. Many of the compounds  
467 detected in this work were also observed in previous isoprene-NO<sub>3</sub> systems (Kwan et al., 2012; Ng et al., 2008;  
468 Schwantes et al., 2015). In this work, only closed-shell products are considered for analysis.



469

470 **Figure 2: Averaged mass spectra for isoprene-NO<sub>3</sub> experiment on 8 August, 2018. Molecular formulas were**  
 471 **determined according to the accurate mass data provided by HR-ToF-CIMS.**

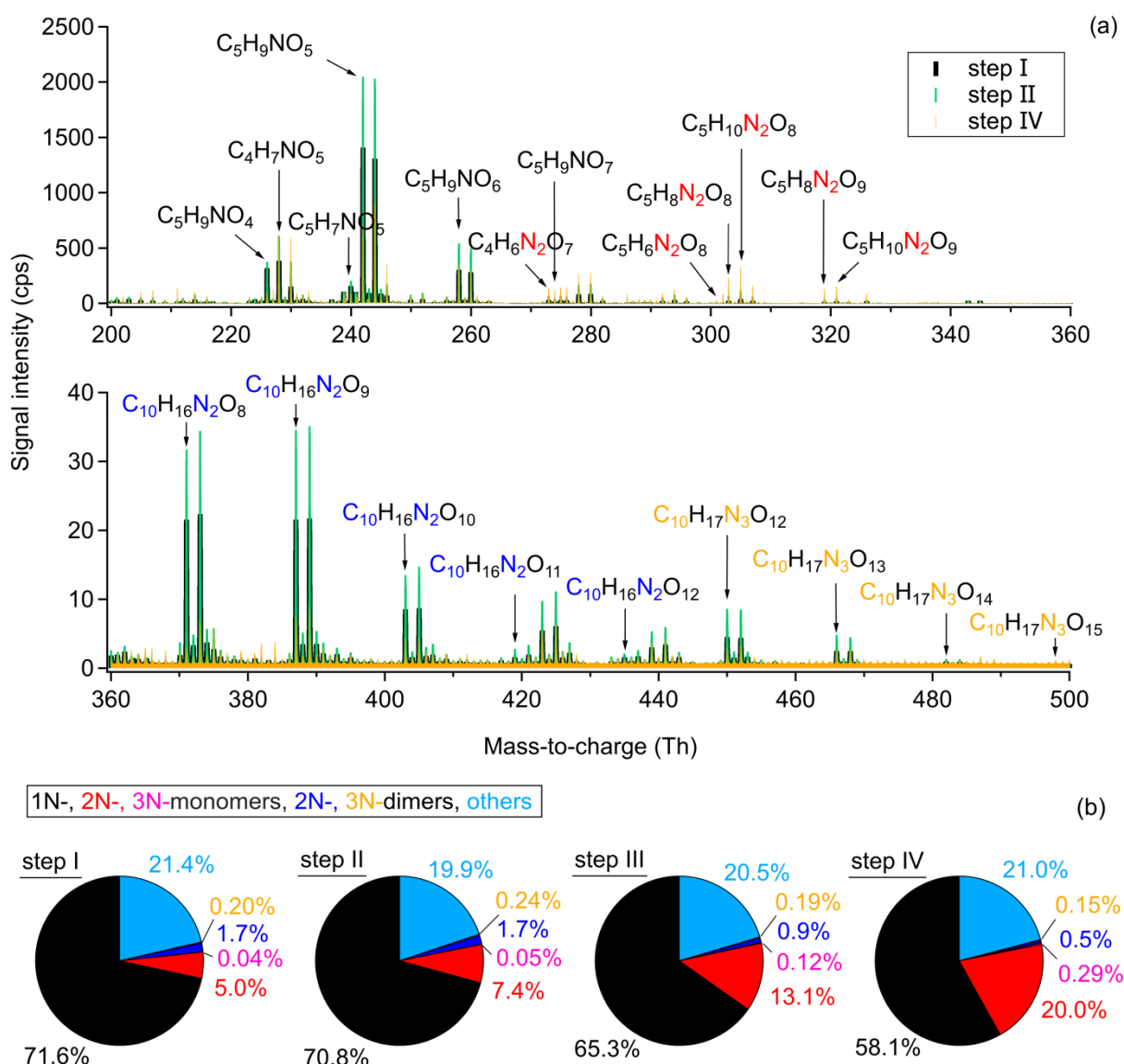
472 The 1N-monomer C<sub>5</sub>H<sub>9</sub>NO<sub>5</sub> at *m/z* 242 is the dominant product formed from the NO<sub>3</sub>-induced isoprene  
 473 oxidation in our experiment, followed by the 1N-decomposition product C<sub>4</sub>H<sub>7</sub>NO<sub>5</sub> at *m/z* 228. In addition to  
 474 C<sub>5</sub>H<sub>9</sub>NO<sub>5</sub>, several analogues with molecular formulas C<sub>5</sub>H<sub>7</sub>NO<sub>4-7</sub> and C<sub>5</sub>H<sub>9</sub>NO<sub>4</sub> are in relatively high abundance.  
 475 C<sub>5</sub>H<sub>8,10</sub>N<sub>2</sub>O<sub>8,9</sub> and C<sub>5</sub>H<sub>9</sub>N<sub>3</sub>O<sub>10-12</sub> are the major 2N- and 3N-monomers. Their signal intensities are one to two  
 476 orders of magnitude lower than those of 1N-monomers. According to the chemical composition, the 1N-  
 477 monomers are likely to be the first-generation products from NO<sub>3</sub> oxidation of isoprene, while the 2N- and 3N-  
 478 monomers probably arise from the further oxidation of 1N-monomers by NO<sub>3</sub>, which therefore should be  
 479 second- or later-generation products. As mentioned before, the reaction of nitrooxy alkylperoxy radicals with  
 480 NO<sub>2</sub> can lead to the formation of peroxy nitrates (for the special case peroxyacyl nitrates, PAN-like) containing  
 481 two N atoms. The peroxy nitrates will decompose rapidly under experimental conditions, whereas the PAN-like  
 482 compounds are more stable (with lifetimes ranging from minutes to weeks at 298K and ambient temperature).  
 483 Such C<sub>5</sub> PAN-like compounds are isomers of aforementioned 2N-monomers, but ought to be first-generation  
 484 products. In addition to C<sub>5</sub>-2N-monomers, we observe some C<sub>4</sub>-2N-monomers with relatively high intensity,  
 485 such as C<sub>4</sub>H<sub>6</sub>N<sub>2</sub>O<sub>7</sub> at *m/z* 273 and C<sub>4</sub>H<sub>8</sub>N<sub>2</sub>O<sub>8</sub> at *m/z* 291. It is proposed that such C<sub>4</sub> dinitrates originate from the  
 486 further oxidation of C<sub>5</sub> carbonyl compounds followed by unimolecular decomposition (Schwantes et al., 2015;  
 487 Wennberg et al., 2018), as shown in Scheme S11.

488 2N-Dimers are C<sub>10</sub> compounds with 8-12 oxygen atoms (C<sub>10</sub>H<sub>16</sub>N<sub>2</sub>O<sub>8-12</sub>), and their signal intensities are  
 489 relatively low compared to that of monomers, approximately three orders of magnitude lower. They might be  
 490 ROOR products from the self or cross reaction of two nitrooxy peroxy radicals (Berndt et al., 2018). 3N-Dimers  
 491 are molecules consisting of 12–16 oxygen atoms (C<sub>10</sub>H<sub>17</sub>N<sub>3</sub>O<sub>12-16</sub>). They are probably formed from further  
 492 oxidation of 2N-dimers or from the cross reaction of a nitrooxy peroxy radical with a dinitrooxy peroxy radicals.

493 **3.2 Multi-generation chemistry**

494 **3.2.1 Molecular composition for each step**

495 As mentioned in Sect. 2.2, there were four injections during the experiment on 8 August (denoted as step I, II,  
 496 III, IV in Fig. 3), wherein in the first three injections all components, O<sub>3</sub>, NO<sub>2</sub>, and isoprene, were added, while  
 497 in the last step only O<sub>3</sub> and NO<sub>2</sub> were injected to promote the further oxidation of early-generation products. The  
 498 extended oxidation time with reinjection of oxidants provides the opportunity to investigate the multi-generation  
 499 oxidation chemistry of isoprene-NO<sub>3</sub> system. The mass spectra show only slow changes in the concentrations  
 500 during the last period of each step, indicating weak chemical evolution. Therefore, we use integrated mass  
 501 spectra over the last 10 minutes of each step for further analysis. Due to the similarity of the integrated mass  
 502 spectra for step II and step III, the latter is omitted in Fig. 3.



503  
 504 **Figure 3: Comparison of the chemical composition of each oxidation step. (A) Averaged mass spectra for step I, II,**  
 505 **and IV, with the omitted spectrum of step III being very similar to that of step II. (B) Relative contribution of**  
 506 **different chemical groups for each oxidation step. Only organic products were counted for analysis. ‘Others’ refers to**  
 507 **CHO compounds without containing nitrogen atoms (e.g., C<sub>5</sub>H<sub>8</sub>O<sub>2</sub> and C<sub>5</sub>H<sub>8</sub>O<sub>3</sub>).**



508 As shown in Fig. 3a, large amounts of 1N-monomers were formed from NO<sub>3</sub> oxidation of isoprene in step I,  
509 wherein C<sub>5</sub>H<sub>9</sub>NO<sub>5</sub>, C<sub>5</sub>H<sub>9</sub>NO<sub>6</sub>, and C<sub>4</sub>H<sub>7</sub>NO<sub>5</sub> are the most abundant compounds in signal. The 2N-monomers,  
510 which are expected from further oxidation of 1N-monomers, are much less compared to 1N-monomers,  
511 accounting for 5.0% of the total organic signals, with the 3N-monomers even less (0.04%). The low  
512 contributions of second-generation products probably results from the relatively high concentration of isoprene  
513 in step I, reducing the possibility for further oxidation of first-generation products. These results indicate that the  
514 system is dominated by first-generation chemistry at the early stage and therefore the oxidation state of products  
515 is low. In addition to monomers, some 2N- and 3N-dimers are observed. They contribute 1.7% and 0.2%,  
516 respectively, to the total organic signals, as shown in Fig. 3b. The low signal intensity of dimers probably results  
517 from their small yield under our experimental conditions. In this case their contribution to SOA formation might  
518 be small. However, a part of the dimers condense onto chamber wall due to their low volatility, so only a  
519 smaller portion exists in the gas phase (compare Table S3 and Fig. S6S5).

520 In step II, the secondary chemistry was accelerated by further addition of O<sub>3</sub> and NO<sub>2</sub>, but the primary  
521 chemistry was also maintained by isoprene injection. As a result, more 1N-monomers (e.g. C<sub>5</sub>H<sub>9</sub>NO<sub>4,5,6</sub>) were  
522 formed compared to step I, as well as dimers (e.g., C<sub>10</sub>H<sub>16</sub>N<sub>2</sub>O<sub>8,9,10</sub> and C<sub>10</sub>H<sub>17</sub>N<sub>3</sub>O<sub>12,13</sub>), as shown in Fig. 3a. The  
523 signals of 2N-monomers almost double in this period compared to those in step I, and their relative contribution  
524 increase from 5.0% to 7.4%. This is attributed to the further oxidation of first-generation products formed in  
525 step I. The relative contributions of different chemical groups exhibited in Fig. 3b clearly show that, although  
526 NO<sub>3</sub> produced from the second addition of NO<sub>2</sub> and O<sub>3</sub> still primarily reacted with newly-injected isoprene,  
527 reaction of NO<sub>3</sub> with the first-generation oxidation products retaining a double bond was inevitable, leading to  
528 more second-generation 2N- or 3N-products compared to step I. The visibly increasing fraction of 2N-  
529 monomers indicates that the second-generation chemistry started to play a more important role than that in the  
530 early stage. In step III, the chemical process proceeded similarly, and thus is not further discussed here.

531 Due to the favorable conditions for further oxidation, the signals of 1N-monomers (such as C<sub>5</sub>H<sub>9</sub>NO<sub>4</sub>,  
532 C<sub>5</sub>H<sub>9</sub>NO<sub>5</sub>, and C<sub>5</sub>H<sub>9</sub>NO<sub>6</sub>), as well as 2N- and 3N-dimers, dropped dramatically in step IV, with their relative  
533 contributions decreasing to 58.1%, 0.5%, and 0.15%, respectively. The decrease in signals of dimers is primarily  
534 ascribed to lack of isoprene, as there were less peroxy radicals under this condition, and hence less dimers were  
535 formed. In addition, their condensation on the wall and dilution also contributed to the decreasing signals.  
536 Furthermore, dimers with 2 or 3 nitrogen atoms possess at least one double bond in their molecular structures  
537 and can thus be further oxidized under high NO<sub>3</sub> condition to form 4N- or 5N-dimers. However, only few 4N-  
538 dimers and no 5N-dimers were detected by CIMS, suggesting that the 4N- and 5N-dimers were either not  
539 formed, or if present, with lower absolute concentrations below the detection limit (approximately 5×10<sup>7</sup> and  
540 5×10<sup>5</sup> molecules cm<sup>-3</sup> for salicylic acid and acetic acid, for an integration time of 60 s). condensed on the wall  
541 due to their low volatilities. In contrast, 2N- and 3N-monomers increase significantly, with their relative  
542 contributions ascending to 20.0% and 0.29%, respectively. This indicates that 2N- and 3N-monomers might be  
543 second- or later-generation products that are formed from the further oxidation of first-generation products.  
544 Additionally, unlike the C<sub>5</sub> monomers, the signal of C<sub>4</sub>H<sub>7</sub>NO<sub>5</sub> increased in step IV, indicating that there is a new  
545 formation pathway for C<sub>4</sub>H<sub>7</sub>NO<sub>5</sub> under excess NO<sub>3</sub> condition. No double bond can remain in such products, as  
546 otherwise they would be oxidized and their signal should decay instead.

547 In summary, above findings confirm that multi-generation chemistry happened during the NO<sub>3</sub>-initiated  
548 isoprene oxidation, and that the later generation oxidation was promoted by “excess” NO<sub>3</sub> radicals.

### 549 3.2.2 Carbon oxidation state ( $\overline{OS}_C$ )

550 The oxidation state of carbon ( $\overline{OS}_C$ ) is defined as the charge a carbon atom takes with assumption that it loses  
551 completely all electrons in bonds to more electronegative atoms and vice versa (Kroll et al., 2011). This quantity  
552 is a metric for the degree of oxidation and will increase with oxidation. Moreover,  $\overline{OS}_C$  together with carbon  
553 number can be used to constrain the composition of organic mixtures and provide insights into their evolutions.  
554 The carbon oxidation state of a species is determined by the relative abundances and oxidation states of non-  
555 carbon atoms in the compound. Since we observed nitrate groups in the products,  $\overline{OS}_C$  is defined by Eq. (3). In  
556 this study, the group-averaged  $\overline{OS}_C$  is the signal-weighted mean average carbon oxidation state of compounds  
557 with the same carbon number, and the bulk-averaged  $\overline{OS}_C$  is the signal-weighted mean average carbon oxidation  
558 state of all detected compounds in the system.

$$559 \overline{OS}_C = \frac{2 \times n_O - n_H - 5 \times n_N}{n_C} \quad (3)$$

560 wherein,  $n_O$ ,  $n_H$ , and  $n_N$  are the number of the respective atoms in the molecular formula.

561 Figure 4 shows the distribution of gas-phase products from the isoprene-NO<sub>3</sub> system in the oxidation state  
562 versus carbon number ( $OS_C$  vs  $n_C$ ) space. The bulk-averaged  $\overline{OS}_C$  is -0.35 in step I, wherein the smaller  
563 molecules ( $C_{\leq 4}$ ) have higher oxidation states than the larger molecules. The group-averaged oxidation state of  
564 C<sub>5</sub> compounds is relatively low ( $\overline{OS}_{C=5} = -0.66$ ), indicating that both of the oxidation and autoxidation degree of  
565 isoprene are quite low during this period. This is consistent with the conclusion made previously from mass  
566 spectra results that at the early stage isoprene-NO<sub>3</sub> oxidation was dominated by first-generation chemistry.

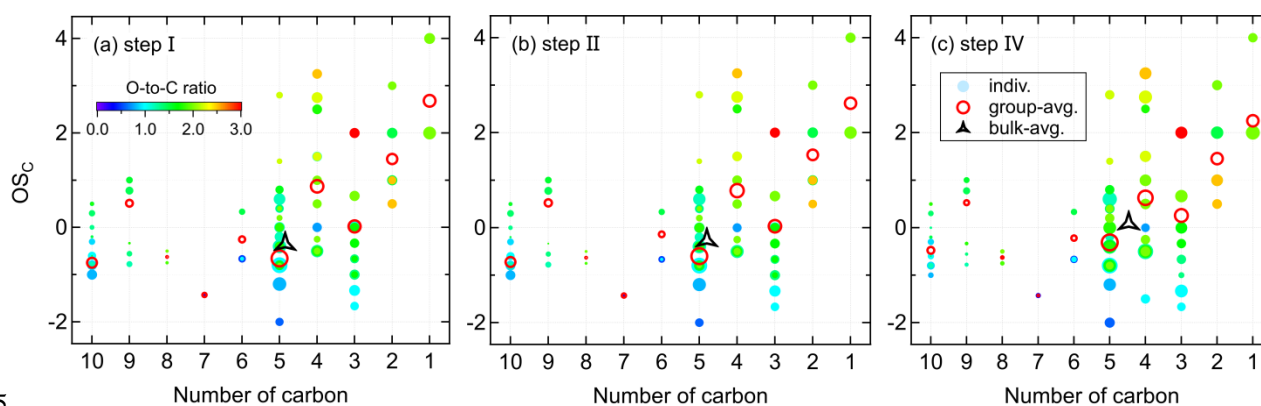
567 The system  $\overline{OS}_C$  increases to -0.26 in step II, confirming that first-generation products were further  
568 oxidized after the second injection. During this step, the  $\overline{OS}_C$  of most compound groups increase only weakly,  
569 except for that of the C<sub>5</sub> compounds. The group-averaged  $\overline{OS}_C$  of C<sub>5</sub> compounds increases to -0.60 in step II,  
570 which is the major contributor to the increase of  $\overline{OS}_C$  of the whole system. The increase of  $\overline{OS}_C$  of C<sub>5</sub>  
571 compounds is largely attributed to the formation of 2N-monomers expected from further oxidation of existing  
572 1N-products formed in step I. This is confirmed by the detectable increase of 2N- and 3N-monomers in the mass  
573 spectra and their higher relative contributions to total signals (see Fig. 3). In addition to C<sub>5</sub> compounds, the  $\overline{OS}_C$   
574 of C<sub>3</sub> and C<sub>6</sub> products increase significantly in step II.

575 In step IV, the secondary oxidation was largely accelerated by reinjection of O<sub>3</sub> and NO<sub>2</sub>, and hence the  
576 system oxidation degree increases, with the bulk-averaged  $\overline{OS}_C$  growing substantially to 0.09. Similarly, the  
577 significant increase of system  $\overline{OS}_C$  is mainly attributed to the C<sub>5</sub> compounds, with their group-averaged  $\overline{OS}_C$   
578 increasing to -0.31. In addition, the  $\overline{OS}_C$  of C<sub>10</sub> compounds increased evidently despite their decreasing signals,  
579 suggesting C<sub>10</sub> dimers were further oxidized as well in step IV. It is worth noting that the average carbon  
580 number decreases step by step with increasing  $\overline{OS}_C$ . This is the case because fewer C<sub>10</sub> products, but more  
581 fragments were formed with the reaction proceeding, as shown in Fig.4 by the decreasing peak areas of larger  
582 molecules but converse trend for smaller molecules. One conceivable explanation for the decreasing dimers but  
583 increasing fragments with the increasing  $\overline{OS}_C$  is that, with more highly oxidized RO<sub>2</sub> formed under high NO<sub>3</sub>

584 condition, the prevailing fate of RO<sub>2</sub> changes from dimerization to forming alkoxy radicals, which would  
585 undergo unimolecular decomposition rapidly, especially when there is a neighboring oxygen-containing  
586 functional group (Molteni et al., 2019).

587 In the oxidation system, the increase in  $\overline{OS}_C$  is attributed to the formation of bonds between carbon and  
588 oxygen as well as other electronegative atoms, and/ or the breaking of bonds between carbon and hydrogen and  
589 other electropositive atoms (Kroll et al., 2011). The -ONO<sub>2</sub> group has an oxidation state of -1, which means that  
590 addition of a -ONO<sub>2</sub> group to isoprene will increase its  $OS_C$  by 0.2. According to our estimates, the values of  
591 system  $\overline{OS}_C$  increased by 1.25 (step I), 0.09 (step II), and 0.35 (step IV), indicating that the increases in  $\overline{OS}_C$  are  
592 not only due to addition of -ONO<sub>2</sub> group(s) but also to other oxygen-containing functionalities. In addition to  
593 functionalization, it is possible that other reactions such as fragmentation and oligomerization which can  
594 increase or reduce the oxidation state were involved during the reaction.

595 As mentioned above, the average carbon oxidation state of a mixture of molecules largely depends on its  
596 chemical composition. Therefore, for different oxidation systems, their  $\overline{OS}_C$  may differ due to different  
597 precursors and oxidation conditions. In our study, the  $\overline{OS}_C$  of NO<sub>3</sub>-initiated isoprene oxidation system increased  
598 from -0.35 to 0.09 with further oxidation. For OH- and O<sub>3</sub>-initiated systems, the average oxidation state of  
599 laboratory-generated isoprene SOA are reported to range from -1.3 to -0.2, as listed in Table S4. It seems that  
600 the SOA generated from chloride-initiated oxidation of isoprene is more oxidized compared to other isoprene  
601 oxidation systems, for which the  $\overline{OS}_C$  can be as high as +1.8 according to limited studies (Wang and Ruiz, 2017).  
602 With regard to ambient measurements, the calculated  $\overline{OS}_C$  values of organic aerosol and aerosol fractions fell  
603 into a wider range between -2 to +2, depending on the site position and the corresponding oxidation  
604 environment of that site (Table S4).



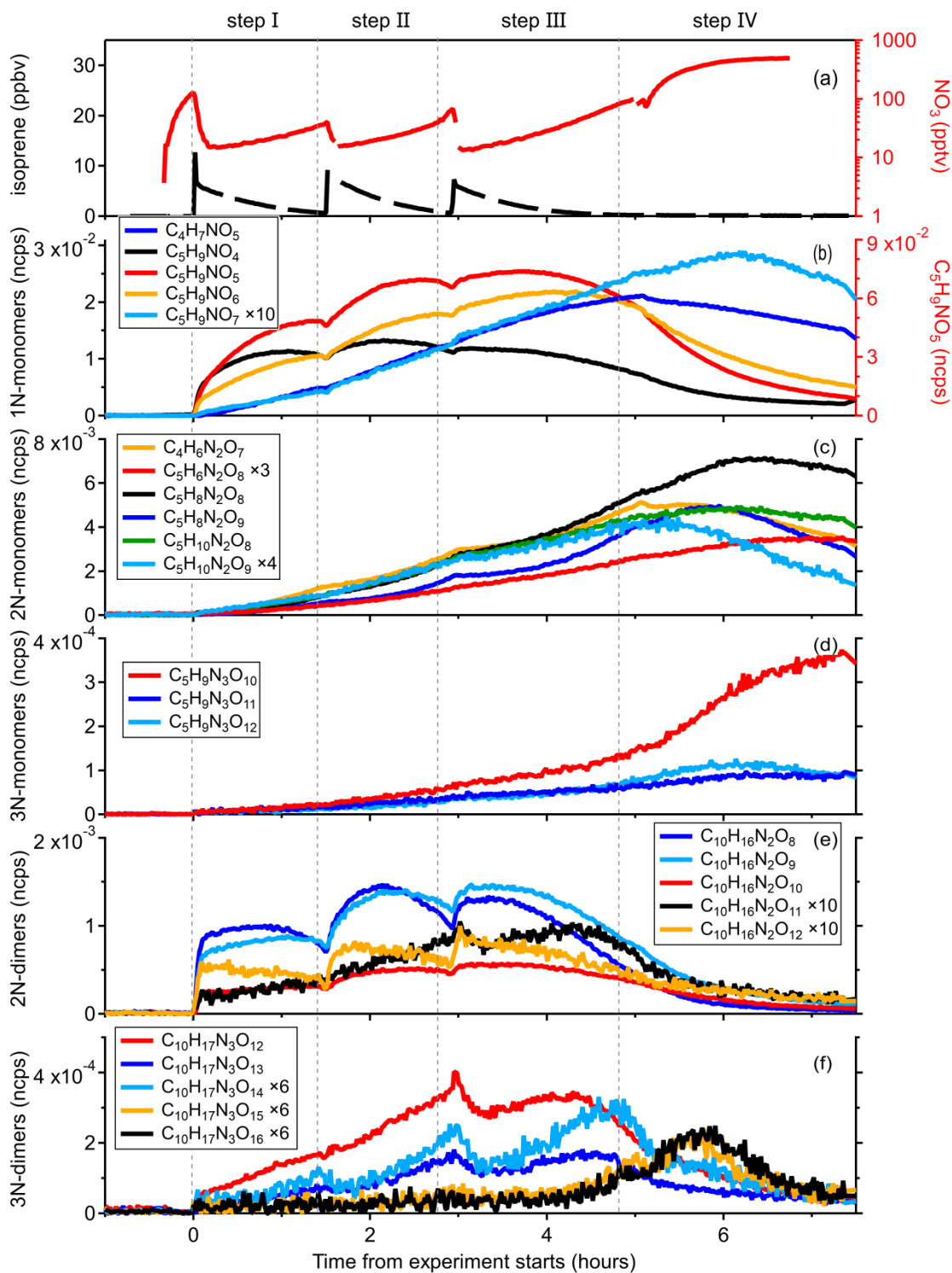
605 **Figure 4: Distribution of gas-phase products from isoprene oxidation by NO<sub>3</sub> in the carbon oxidation state ( $OS_C$ )**  
606 **versus carbon number ( $n_C$ ) space. Markers are colored by oxygen-to-carbon molar ratio and sized by the logarithm**  
607 **of peak areas. The group-averaged and bulk-averaged  $\overline{OS}_C$  are signal-weighted mean average carbon oxidation state**  
608 **of compounds with the same carbon number and of all detected compounds, respectively.**  
609

610 In summary, isoprene and its products undergo further oxidation by NO<sub>3</sub>, leading to an increase in degree  
611 of oxidation of products as the reaction proceeds. The increasing bulk  $\overline{OS}_C$  is largely governed by the highly  
612 oxidized C<sub>5</sub> compounds. In addition, more fragments but fewer dimers are formed as the  $\overline{OS}_C$  increases, which  
613 can be probably explained by the change of RO<sub>2</sub> fate from prevailing dimerization to fragmentation through the  
614 alkoxy radical channel.

### 615 3.2.3 Characteristics of different-generation products

#### 616 (1) 1N-monomers

617 To illustrate the multi-generation chemistry involved in the isoprene-NO<sub>3</sub> reaction system, Fig. 5 shows the time  
618 evolution of the major gas-phase products. The signal of the most abundant compounds, C<sub>5</sub>H<sub>9</sub>NO<sub>5</sub>, increases  
619 rapidly as soon as the reaction was initiated, reaching a maximum when its chemical production rate matches its  
620 loss rate (including chemical destruction, wall loss, dilution, etc.), and decreases slowly thereafter. Its time  
621 behavior in the first three steps is similar. In step IV, however, the injection of O<sub>3</sub> and NO<sub>2</sub> resulted in a strong  
622 decay of C<sub>5</sub>H<sub>9</sub>NO<sub>5</sub>, owing to the occurrence of further oxidation by NO<sub>3</sub>. The time behavior suggests that  
623 C<sub>5</sub>H<sub>9</sub>NO<sub>5</sub> signal is dominated by first-generation oxidation products, and the same conclusion can be made for  
624 C<sub>5</sub>H<sub>9</sub>NO<sub>4</sub> and C<sub>5</sub>H<sub>9</sub>NO<sub>6</sub>. According to the mechanistic framework developed above, the C<sub>5</sub>H<sub>9</sub>NO<sub>4</sub>, C<sub>5</sub>H<sub>9</sub>NO<sub>5</sub>,  
625 and C<sub>5</sub>H<sub>9</sub>NO<sub>6</sub> compounds most likely correspond to hydroxyl nitrates, nitrooxy hydroperoxides, and hydroxy  
626 hydroperoxy nitrates, respectively, but other constitutional isomers are possible. They were already observed in  
627 previous studies and were proposed to form through reactions of INO<sub>2</sub> radicals with RO<sub>2</sub>, HO<sub>2</sub>, and  
628 unimolecular rearrangement, as shown in Scheme S5 (Ng et al., 2008; Kwan et al., 2012; Schwantes et al., 2015;  
629 Wennberg et al., 2018).



630

631 **Figure 5: Time evolution of selected gas-phase compounds measured during the isoprene - NO<sub>3</sub> experiment on 08**  
 632 **August, 2018. (a) Time series of O<sub>3</sub>, NO<sub>2</sub>, NO<sub>3</sub> and isoprene. (b)–(f) Time evolution of major 1N-monomers (C<sub>5</sub>H<sub>9</sub>NO<sub>4-7</sub>**  
 633 **and C<sub>4</sub>H<sub>7</sub>NO<sub>5</sub>), 2N-monomers (C<sub>4</sub>H<sub>6</sub>N<sub>2</sub>O<sub>7</sub>, C<sub>5</sub>H<sub>6</sub>N<sub>2</sub>O<sub>8</sub>, and C<sub>5</sub>H<sub>8,10</sub>N<sub>2</sub>O<sub>8,9</sub>), 3N-monomers (C<sub>5</sub>H<sub>9</sub>N<sub>3</sub>O<sub>10-12</sub>), 2N-dimers**  
 634 **(C<sub>10</sub>H<sub>16</sub>N<sub>2</sub>O<sub>8-12</sub>), and 3N-dimers (C<sub>10</sub>H<sub>17</sub>N<sub>3</sub>O<sub>12-16</sub>).**

635

636

637

638

As shown in Fig. 5b, the temporal evolution of C<sub>5</sub>H<sub>9</sub>NO<sub>7</sub> (*m/z* 274) is different to C<sub>5</sub>H<sub>9</sub>NO<sub>4-6</sub> compounds, suggesting that it has a completely different formation pathway. Specifically, the formation rate of C<sub>5</sub>H<sub>9</sub>NO<sub>7</sub> is initially much slower than that of C<sub>5</sub>H<sub>9</sub>NO<sub>4-6</sub> but accelerates to become comparable to them later as the experiment proceeds, i.e. when a multitude of first-generation products are accumulated. This implies that

639 C<sub>5</sub>H<sub>9</sub>NO<sub>7</sub> is produced from the further oxidation of first-generation products, and its signal is dominated by  
640 second-generation products. Based on its molecular composition, C<sub>5</sub>H<sub>9</sub>NO<sub>7</sub> could be the dihydroperoxy nitrate  
641 as shown in Scheme S5, but its formation through the reaction of HO<sub>2</sub> with nitrooxy hydroperoxy radical from  
642 INO<sub>2</sub> autoxidation suggests it should be first-generation products, not in accordance with the time behavior we  
643 actually observe. Consequently, we can conclude that it is not the major formation pathway that contributed to  
644 C<sub>5</sub>H<sub>9</sub>NO<sub>7</sub> observed in this study. As shown in Scheme S7, the first-generation C<sub>5</sub> hydroxy carbonyl (C<sub>5</sub>H<sub>8</sub>O<sub>2</sub>,  
645 *m/z* 179) can be further oxidized by NO<sub>3</sub> and the resulting alkyl radical would rapidly recombine with O<sub>2</sub>,  
646 producing a new peroxy radical, which then reacts with HO<sub>2</sub> radicals to form C<sub>5</sub>H<sub>9</sub>NO<sub>7</sub> (hydroxy hydroperoxy  
647 carbonyl nitrate). Similarly, the C<sub>5</sub> hydroperoxy carbonyl (C<sub>5</sub>H<sub>8</sub>O<sub>3</sub>, *m/z* 195) can also lead to the formation of  
648 such C<sub>5</sub>H<sub>9</sub>NO<sub>7</sub> (isomer of that formed through C<sub>5</sub>H<sub>8</sub>O<sub>2</sub> channel) through further oxidation (see Scheme S7).  
649 According to above two mechanisms, C<sub>5</sub>H<sub>9</sub>NO<sub>7</sub> formed following such reaction pathways should be second-  
650 generation products, better consistent with its time behavior.

651 Considering its similar time behavior to C<sub>5</sub>H<sub>9</sub>NO<sub>7</sub>, the observed C<sub>4</sub>H<sub>7</sub>NO<sub>5</sub> (*m/z* 228) signal is likewise  
652 thought to be dominated by second-generation products. Schwantes et al. (2015) proposed such a C<sub>4</sub> product  
653 based on OH-initiated chemistry, but as the OH concentration in our system was ~~close to zero~~below the  
654 detection limit during the experiment (see Fig. S3S2), this formation pathway cannot apply in our situation.  
655 Instead, we suggest that C<sub>4</sub>H<sub>7</sub>NO<sub>5</sub> is formed through the unimolecular decomposition of the C<sub>5</sub> alkoxy or acyl  
656 radicals, which result from further oxidation of the C<sub>5</sub> hydroxy carbonyl (C<sub>5</sub>H<sub>8</sub>O<sub>2</sub>, *m/z* 179), as shown in Scheme  
657 S7. It should be pointed out here that there may be reaction pathways forming C<sub>4</sub>H<sub>7</sub>NO<sub>5</sub> as first-generation  
658 products that are not considered here, whereas it is no doubt that the second-generation chemistry played a  
659 dominant role in C<sub>4</sub>H<sub>7</sub>NO<sub>5</sub> formation according to its time evolution measured by CIMS.

660 Although C<sub>4</sub>H<sub>7</sub>NO<sub>5</sub> and C<sub>5</sub>H<sub>9</sub>NO<sub>7</sub> show similar time behaviors in the first three steps, it seems that they  
661 followed fairly different reaction pathways when the concentration of NO<sub>3</sub> in the chamber increased  
662 dramatically in step IV. As shown in Fig. 5b, the signal of C<sub>4</sub>H<sub>7</sub>NO<sub>5</sub> drops immediately after the injection of O<sub>3</sub>  
663 and NO<sub>2</sub>, while that of C<sub>5</sub>H<sub>9</sub>NO<sub>7</sub> continues to increase, although its formation rate becomes slightly lower with  
664 increasing NO<sub>3</sub> concentration. The decay of C<sub>4</sub>H<sub>7</sub>NO<sub>5</sub> signal can be explained by more chemical destruction or  
665 less production under high NO<sub>3</sub> condition, wherein the latter seems more sensible in terms of its structure (no  
666 double bond remaining). As shown in Scheme S7, the second-generation C<sub>4</sub>H<sub>7</sub>NO<sub>5</sub> and C<sub>5</sub>H<sub>9</sub>NO<sub>7</sub> compounds  
667 share the same precursor in the C<sub>5</sub>H<sub>8</sub>O<sub>2</sub> channel. Consequently, the production of C<sub>5</sub>H<sub>9</sub>NO<sub>7</sub> through this  
668 pathway would be interrupted immediately after the injection of O<sub>3</sub> and NO<sub>2</sub> like C<sub>4</sub>H<sub>7</sub>NO<sub>5</sub>. In reality, its signal  
669 might decay even faster due to the larger reaction rate of RO<sub>2</sub> H-shift (leading to the formation of C<sub>4</sub>H<sub>7</sub>NO<sub>5</sub>)  
670 than that of RO<sub>2</sub> reacting with HO<sub>2</sub> (leading to the formation of C<sub>5</sub>H<sub>9</sub>NO<sub>7</sub>). As presented by Vereecken and  
671 Nozière (2020), the rate coefficient of aldehydic H-shift is  $\geq 0.5 \text{ s}^{-1}$  (298 K), while the pseudo first order rate  
672 coefficient of RO<sub>2</sub> reacting with HO<sub>2</sub> is  $\sim 10^{-3} \text{ s}^{-1}$  ( $k$  (298 K) =  $5 \times 10^{-12} \text{ cm}^3 \text{ molecules}^{-1} \text{ s}^{-1}$  (Atkinson, 2007), and  
673 [HO<sub>2</sub>]  $\sim 4 \times 10^8 \text{ molecules cm}^{-3}$ ), about two orders of magnitude smaller. This result implies that the increasing  
674 C<sub>5</sub>H<sub>9</sub>NO<sub>7</sub> observed is contributed to by other formation pathways. As mentioned before, C<sub>5</sub>H<sub>9</sub>NO<sub>7</sub> can also be  
675 produced by C<sub>5</sub>H<sub>8</sub>O<sub>3</sub> oxidation. We find that the signal of C<sub>4</sub>H<sub>7</sub>NO<sub>6</sub> (*m/z* 244), which results from C<sub>5</sub>H<sub>8</sub>O<sub>3</sub>  
676 oxidation as well, remains increasing after the injection of O<sub>3</sub> and NO<sub>2</sub>. This tentatively confirms that the  
677 production of C<sub>5</sub>H<sub>9</sub>NO<sub>7</sub> in step IV is mainly from C<sub>5</sub>H<sub>8</sub>O<sub>3</sub> oxidation channel. More experimental or theoretical  
678 studies are needed to provide insights into these differences.

679 **(2) 2N- and 3N-monomers**

680 As shown in Fig. 5c, 2N-monomers formed much slower than 1N-monomers in the early stage, but their  
681 formation rates were accelerated in step II and step III, probably due to the accumulation of first-generation  
682 products. According to our mechanistic framework, 2N-monomers are second-generation products resulting  
683 from the further oxidation of 1N-monomers by  $\text{NO}_3$ , which is consistent with their time behaviors detected by  
684 CIMS.

685 Like  $\text{C}_4\text{H}_7\text{NO}_5$  and  $\text{C}_5\text{H}_9\text{NO}_7$ , different 2N-monomers have similar behavior in the first three steps, but they  
686 are obviously different in step IV when the concentration of  $\text{NO}_3$  increased drastically in the chamber. For  
687 instance, the signals of  $\text{C}_5\text{H}_8\text{N}_2\text{O}_8$ ,  $\text{C}_5\text{H}_8\text{N}_2\text{O}_9$  and  $\text{C}_5\text{H}_{10}\text{N}_2\text{O}_8$  continue to increase after the injection of  $\text{O}_3$  and  
688  $\text{NO}_2$ , while that of  $\text{C}_5\text{H}_{10}\text{N}_2\text{O}_9$  drops immediately. This is related to their detailed formation mechanisms which  
689 are outside the scope of this study. Furthermore,  $\text{C}_5\text{H}_8\text{N}_2\text{O}_9$  and  $\text{C}_5\text{H}_{10}\text{N}_2\text{O}_9$  decay a little bit faster than  
690  $\text{C}_5\text{H}_8\text{N}_2\text{O}_8$  and  $\text{C}_5\text{H}_{10}\text{N}_2\text{O}_8$ , which might be related to their volatility and will be further discussed in next section.

691 Different from other 2N-monomers, the signals of  $\text{C}_5\text{H}_6\text{N}_2\text{O}_8$  ( $m/z$  301) increases continuously under high  
692  $\text{NO}_3$  condition, although its net formation rate is almost zero at the end of step IV. The characteristics of  
693  $\text{C}_5\text{H}_6\text{N}_2\text{O}_8$  under high  $\text{NO}_3$  condition reflects its different formation pathways from other dinitrates, and without  
694 having a comprehensive knowledge of its chemical mechanism, we are unable to tell what exactly leads to the  
695 differences. In the Master Chemical Mechanism (MCM v3.3.1),  $\text{C}_5\text{H}_6\text{N}_2\text{O}_8$  is proposed to be a PAN-like  
696 compound stemming from the  $\text{C}_5$  nitroxy carbonyl ( $\text{C}_5\text{H}_7\text{NO}_4$ )  
697 (<http://mcm.leeds.ac.uk/MCM/browse.htm?species=NC4CHO>). Such  $\text{C}_5\text{H}_6\text{N}_2\text{O}_8$  compound would react with  
698  $\text{NO}_3$  radicals due to the remaining double bond, and hence this cannot be the predominant formation pathway of  
699 the  $\text{C}_5\text{H}_6\text{N}_2\text{O}_8$  observed in this study. Based on the formation mechanism of dinitrooxyepoxides ( $\text{C}_5\text{H}_8\text{N}_2\text{O}_7$ )  
700 proposed by Kwan et al. (2012), we suggest that  $\text{C}_5\text{H}_6\text{N}_2\text{O}_8$  can also be a dinitrooxyepoxide resulting from  
701 cyclization of specific hydroperoxy alkyl radicals, as shown in Scheme S10. Alternatively, the  $\text{C}_5$  hydroxy  
702 nitrate ( $\text{C}_5\text{H}_9\text{NO}_4$ ) can be oxidized by  $\text{NO}_3$  and then react with  $\text{NO}_3$  radicals again, forming  $\text{C}_5\text{H}_6\text{N}_2\text{O}_8$  with two  
703 aldehyde groups ultimately (see Scheme S10). According to the proposed mechanisms above,  $\text{C}_5\text{H}_6\text{N}_2\text{O}_8$  formed  
704 through the first two pathways are second-generation products, while those from the third channel are third-  
705 generation products, in accordance with its time behavior measured by CIMS.

706 In addition to  $\text{C}_5$ -2N-monomers, we observe some  $\text{C}_4$  dinitrates such as  $\text{C}_4\text{H}_6\text{N}_2\text{O}_7$  ( $m/z$  273) and  $\text{C}_4\text{H}_8\text{N}_2\text{O}_8$   
707 ( $m/z$  291), and the signal intensity of  $\text{C}_4\text{H}_6\text{N}_2\text{O}_7$  is comparable to the major  $\text{C}_5$ -2N-monomers.  $\text{C}_4$  dinitrates have  
708 rarely been mentioned in previous isoprene- $\text{NO}_3$  studies. As shown in Fig. 5c,  $\text{C}_4\text{H}_6\text{N}_2\text{O}_7$  has similar time  
709 behavior to  $\text{C}_5$ -2N-monomers, and hence is thought to be second-generation products. Wennberg et al. (2018)  
710 proposed that such a  $\text{C}_4$  dinitrate was generated from OH-initiated further oxidation of  $\text{C}_5\text{H}_7\text{NO}_4$ . However, this  
711 is not applicable here due to a lack of OH radicals in our system. Instead, we propose that the  $\text{C}_4\text{H}_6\text{N}_2\text{O}_7$   
712 observed in this study is dinitrooxy carbonyl compound resulting from  $\text{NO}_3$  oxidation of  $\text{C}_5\text{H}_7\text{NO}_4$  with  
713 subsequent unimolecular decomposition (see Scheme S11 for details).

714 As shown in Fig. 5d, 3N-monomers are generated more slowly than 1N-monomers, but their signals grow  
715 gradually as the experiment proceeds, with a significant increase especially for  $\text{C}_5\text{H}_9\text{N}_3\text{O}_{10}$  in the last step.  
716 Furthermore, we can see from Fig. 5c and Fig. 5d that the signals of  $\text{C}_5$  trinitrates in step IV appear  
717 anticorrelated to that of  $\text{C}_5\text{H}_{10}\text{N}_2\text{O}_8$  and  $\text{C}_5\text{H}_{10}\text{N}_2\text{O}_9$ . The gas-phase 3N-monomers have rarely been reported in  
718 previous literature. Ng et al. (2008) observed  $\text{C}_5\text{H}_9\text{N}_3\text{O}_{10}$  compound in the particle-phase and assumed that it

719 was produced from NO<sub>3</sub> oxidation of the C<sub>5</sub> hydroxy nitrate (C<sub>5</sub>H<sub>9</sub>NO<sub>4</sub>). Similarly, C<sub>5</sub>H<sub>9</sub>N<sub>3</sub>O<sub>11</sub> and C<sub>5</sub>H<sub>9</sub>N<sub>3</sub>O<sub>12</sub>  
720 can be formed through NO<sub>3</sub> reacting with dinitrooxy peroxy radicals, which result from corresponding first-  
721 generation nitrooxy compounds (C<sub>5</sub> hydroperoxy nitrate, C<sub>5</sub>H<sub>9</sub>NO<sub>5</sub> or C<sub>5</sub> hydroxy hydroperoxy nitrate, C<sub>5</sub>H<sub>9</sub>NO<sub>6</sub>)  
722 oxidation by NO<sub>3</sub> radicals, as shown in Scheme S12. 3N-Monomers formed following such pathways are  
723 second-generation products by definition. Regarding the rising signals of 3N-monomers in step IV, one  
724 explanation is that although the reaction of dinitrooxy peroxy radicals with NO<sub>3</sub> is not an oxidation process,  
725 their formation can be significantly facilitated by increasing NO<sub>3</sub> concentration. It is also possible that 3N-  
726 monomers are formed through H-abstraction of 2N-monomers. NO<sub>3</sub> radicals can abstract the hydrogen of  
727 dihydroxy dinitrate (C<sub>5</sub>H<sub>10</sub>N<sub>2</sub>O<sub>8</sub>) or hydroxyl hydroperoxy dinitrate (C<sub>5</sub>H<sub>10</sub>N<sub>2</sub>O<sub>9</sub>) from the carbon with an –OH,  
728 –OOH or –ONO<sub>2</sub> group attached, leading to alkyl radicals that can subsequently recombine with O<sub>2</sub> and then  
729 react with NO<sub>2</sub> or NO<sub>3</sub>, yielding trinitrates or peroxytrinitrates containing three nitrogen atoms. 3N-Monomers  
730 stemming from such reactions ought to be third-generation products. However, we should point out that 3N-  
731 monomers formed following H-abstraction pathway are less likely because abstracting hydrogen from the  
732 hydroxyl, hydroperoxy or nitrooxy carbon would lead to fragmentation at most cases (Bianchi et al., 2019).

733 In addition, it is interesting to note that the signal of C<sub>5</sub>H<sub>9</sub>N<sub>3</sub>O<sub>10</sub> increases continuously throughout step IV,  
734 whereas that of C<sub>5</sub>H<sub>9</sub>N<sub>3</sub>O<sub>11</sub> and C<sub>5</sub>H<sub>9</sub>N<sub>3</sub>O<sub>12</sub> drop after a short period of growth. Meanwhile, the production of  
735 C<sub>5</sub>H<sub>9</sub>N<sub>3</sub>O<sub>10</sub> is facilitated by the increasing NO<sub>3</sub> concentration compared to that of C<sub>5</sub>H<sub>9</sub>N<sub>3</sub>O<sub>12</sub> and C<sub>5</sub>H<sub>9</sub>N<sub>3</sub>O<sub>11</sub>.  
736 Currently, we cannot explain what exactly causes these differences, but we suspect that there may be different  
737 chemical pathways forming different 3N-monomers that are not covered here and may also be related to their  
738 different physical properties, such as vapor pressures.

### 739 (3) 2N- and 3N-dimers

740 As shown in Fig. 5e, 2N-dimers (except for C<sub>10</sub>H<sub>16</sub>N<sub>2</sub>O<sub>11</sub>) display very similar time behavior to 1N-monomer,  
741 which form rapidly after each injection, indicating that the signals of 2N-dimers are dominated by first-  
742 generation products like most 1N-monomers. It is noted that the time behavior of C<sub>10</sub>H<sub>16</sub>N<sub>2</sub>O<sub>11</sub> (*m/z* 419) is  
743 completely different from that of other 2N-dimers. As illustrated in Fig. 5e, the production rate of C<sub>10</sub>H<sub>16</sub>N<sub>2</sub>O<sub>11</sub>  
744 is initially much slower compared to other dimers. Besides, its signal increases monotonically in the first two  
745 oxidation stages, whereas that of the others always increase first, approaching the maximum as its chemical  
746 production competes against the losses, and decrease gradually thereafter. The special time behavior of  
747 C<sub>10</sub>H<sub>16</sub>N<sub>2</sub>O<sub>11</sub> suggests that it has a different formation pathway from other 2N-dimers, and its signal is most  
748 likely dominated by secondary products. In addition, we find that the signal of C<sub>10</sub>H<sub>16</sub>N<sub>2</sub>O<sub>12</sub> always starts to  
749 decay earlier than that of C<sub>10</sub>H<sub>16</sub>N<sub>2</sub>O<sub>8</sub> and C<sub>10</sub>H<sub>16</sub>N<sub>2</sub>O<sub>9</sub>. If we assume that their production rates have the same  
750 order of magnitude (confirming by their formation rates after each injection), then it can be concluded that  
751 C<sub>10</sub>H<sub>16</sub>N<sub>2</sub>O<sub>12</sub> had additional chemical destruction, or its volatility is much lower than C<sub>10</sub>H<sub>16</sub>N<sub>2</sub>O<sub>8</sub> and  
752 C<sub>10</sub>H<sub>16</sub>N<sub>2</sub>O<sub>9</sub> and hence has more rapid lost on the wall. It seems the second hypothesis is more likely when  
753 comparing its signal with and without dilution and wall-loss corrections (see Fig. S4S5). More detailed  
754 discussion about volatilities of different isoprene organonitrates will be provided in the next section.

755 It is proposed that dimers (ROOR') are likely formed through the self- or cross-reaction of two peroxy  
756 radicals (Berndt et al. 2018). Consequently, the generation number of dimers depends only on how the involved  
757 peroxy radicals are formed. Table S1 summarizes the possible permutation scheme of 2N-dimers from RO<sub>2</sub> +



758 RO<sub>2</sub> reactions, and their structural information can be found in Scheme S13. For example, self-reaction of two  
759 C<sub>5</sub> nitrooxy peroxy radicals (C<sub>5</sub>H<sub>8</sub>NO<sub>5</sub>) leads to the formation of C<sub>10</sub>H<sub>16</sub>N<sub>2</sub>O<sub>8</sub> compound, while recombination  
760 of two C<sub>5</sub> nitrooxy hydroxyl peroxy radicals (C<sub>5</sub>H<sub>8</sub>NO<sub>6</sub>) or a C<sub>5</sub> nitrooxy peroxy radical (C<sub>5</sub>H<sub>8</sub>NO<sub>5</sub>) with a C<sub>5</sub>  
761 nitrooxy hydroperoxy peroxy radical (C<sub>5</sub>H<sub>8</sub>NO<sub>7</sub>) results in C<sub>10</sub>H<sub>16</sub>N<sub>2</sub>O<sub>10</sub> compound. According to their time  
762 behavior, 2N-dimers (except for C<sub>10</sub>H<sub>16</sub>N<sub>2</sub>O<sub>11</sub>) are thought to be first-generation products, and from this fact we  
763 can infer that the peroxy radicals contributing to dimer formation are dominated by first-generation  
764 intermediates. With regard to C<sub>10</sub>H<sub>16</sub>N<sub>2</sub>O<sub>11</sub>, we conclude that it is most likely a secondary product considering  
765 its typical second-generation behavior. In other words, at least one of the two C<sub>5</sub> nitrooxy peroxy radicals  
766 involved in formation of C<sub>10</sub>H<sub>16</sub>N<sub>2</sub>O<sub>11</sub> must be a secondary intermediate. As listed in Table S1, C<sub>10</sub>H<sub>16</sub>N<sub>2</sub>O<sub>11</sub> can  
767 be formed through C<sub>5</sub>H<sub>8</sub>NO<sub>6</sub> + C<sub>5</sub>H<sub>8</sub>NO<sub>7</sub> or C<sub>5</sub>H<sub>8</sub>NO<sub>6</sub> + C<sub>5</sub>H<sub>8</sub>NO<sub>7</sub> reactions, wherein C<sub>5</sub>H<sub>8</sub>NO<sub>7</sub> and C<sub>5</sub>H<sub>8</sub>NO<sub>8</sub>  
768 would be secondary peroxy radicals if they are formed through NO<sub>3</sub> further oxidation of the C<sub>5</sub> hydroxy  
769 carbonyl compounds (C<sub>5</sub>H<sub>8</sub>O<sub>2</sub> or C<sub>5</sub>H<sub>8</sub>O<sub>3</sub>), as shown in Scheme S7. In addition, it is possible that C<sub>10</sub>H<sub>16</sub>N<sub>2</sub>O<sub>11</sub> is  
770 formed from a C<sub>5</sub> hydroxy peroxy radical C<sub>5</sub>H<sub>9</sub>O<sub>3</sub> reacting with a C<sub>5</sub> dinitrooxy hydroxy carbonyl peroxy radical  
771 C<sub>5</sub>H<sub>7</sub>N<sub>2</sub>O<sub>10</sub> (from C<sub>5</sub>H<sub>7</sub>NO<sub>5</sub> oxidation by NO<sub>3</sub>), as we observe high abundant C<sub>5</sub>H<sub>10</sub>O<sub>3</sub> during the experiment,  
772 although C<sub>5</sub>H<sub>10</sub>O<sub>3</sub> is assumed to be the major product of the OH-initiated chemistry.

773 Apart from 2N-dimers, we observe detectable signals at *m/z* 450, 466, 482, 498 and 514, which are  
774 identified as 3N-dimers with molecular formulas C<sub>10</sub>H<sub>17</sub>N<sub>3</sub>O<sub>12-16</sub>. C<sub>10</sub>H<sub>17</sub>N<sub>3</sub>O<sub>12</sub> and C<sub>10</sub>H<sub>17</sub>N<sub>3</sub>O<sub>13</sub> were detected  
775 in the particle-phase in previous study, suggesting that they have low volatility and can contribute to SOA  
776 formation (Ng et al., 2008). As shown in Fig. 5f, 3N-dimers form much slower than 2N-dimers, but their  
777 productions are accelerated as the experiment proceeds. This is similar to the characteristics of second-  
778 generation 2N- and 3N-monomers to some degree, suggesting that the signals of 3N-dimers we observed are  
779 most likely dominated by secondary or even later-generation compounds.

780 It is worth noting that C<sub>10</sub>H<sub>17</sub>N<sub>3</sub>O<sub>12-14</sub> and C<sub>10</sub>H<sub>17</sub>N<sub>3</sub>O<sub>15,16</sub> have two completely different types of time  
781 behavior. The signals of C<sub>10</sub>H<sub>17</sub>N<sub>3</sub>O<sub>12</sub>, C<sub>10</sub>H<sub>17</sub>N<sub>3</sub>O<sub>13</sub> and C<sub>10</sub>H<sub>17</sub>N<sub>3</sub>O<sub>14</sub> more or less increase in the first three  
782 oxidation steps and start to decline in the late of step III with increasing NO<sub>3</sub> concentration. As depicted in  
783 Scheme S13, 3N-dimers can result from further oxidation of 2N-dimers or the cross-reaction of a first-  
784 generation nitrooxy peroxy radical with a secondary dinitrooxy peroxy radical. Accordingly, such 3N-dimers are  
785 thought to be second-generation products, and they would further react with NO<sub>3</sub> due to the remaining double  
786 bond in their molecular structure, leading to severe chemical destruction of these compounds under high NO<sub>3</sub>  
787 condition. This is consistent with the time behavior of C<sub>10</sub>H<sub>17</sub>N<sub>3</sub>O<sub>12</sub>, C<sub>10</sub>H<sub>17</sub>N<sub>3</sub>O<sub>13</sub> and C<sub>10</sub>H<sub>17</sub>N<sub>3</sub>O<sub>14</sub>. In contrast,  
788 C<sub>10</sub>H<sub>17</sub>N<sub>3</sub>O<sub>15</sub> and C<sub>10</sub>H<sub>17</sub>N<sub>3</sub>O<sub>16</sub> are formed even more slowly, and their production in the first four hours is close  
789 to zero. However, their signals start to climb in the late of step III, during which that of C<sub>10</sub>H<sub>17</sub>N<sub>3</sub>O<sub>12</sub>,  
790 C<sub>10</sub>H<sub>17</sub>N<sub>3</sub>O<sub>13</sub> and C<sub>10</sub>H<sub>17</sub>N<sub>3</sub>O<sub>14</sub> decline. This suggests that C<sub>10</sub>H<sub>17</sub>N<sub>3</sub>O<sub>15</sub> and C<sub>10</sub>H<sub>17</sub>N<sub>3</sub>O<sub>16</sub> formed under high NO<sub>3</sub>  
791 condition probably result from further reactions of C<sub>10</sub>H<sub>17</sub>N<sub>3</sub>O<sub>12-14</sub>. However, this assumption is highly uncertain  
792 and more experimental and theoretical studies are needed to substantiate it. In terms of their time behavior,  
793 C<sub>10</sub>H<sub>17</sub>N<sub>3</sub>O<sub>15</sub> and C<sub>10</sub>H<sub>17</sub>N<sub>3</sub>O<sub>16</sub> are thought to be third- or even later-generation products.

### 794 3.3 Volatility distribution of isoprene nitrates

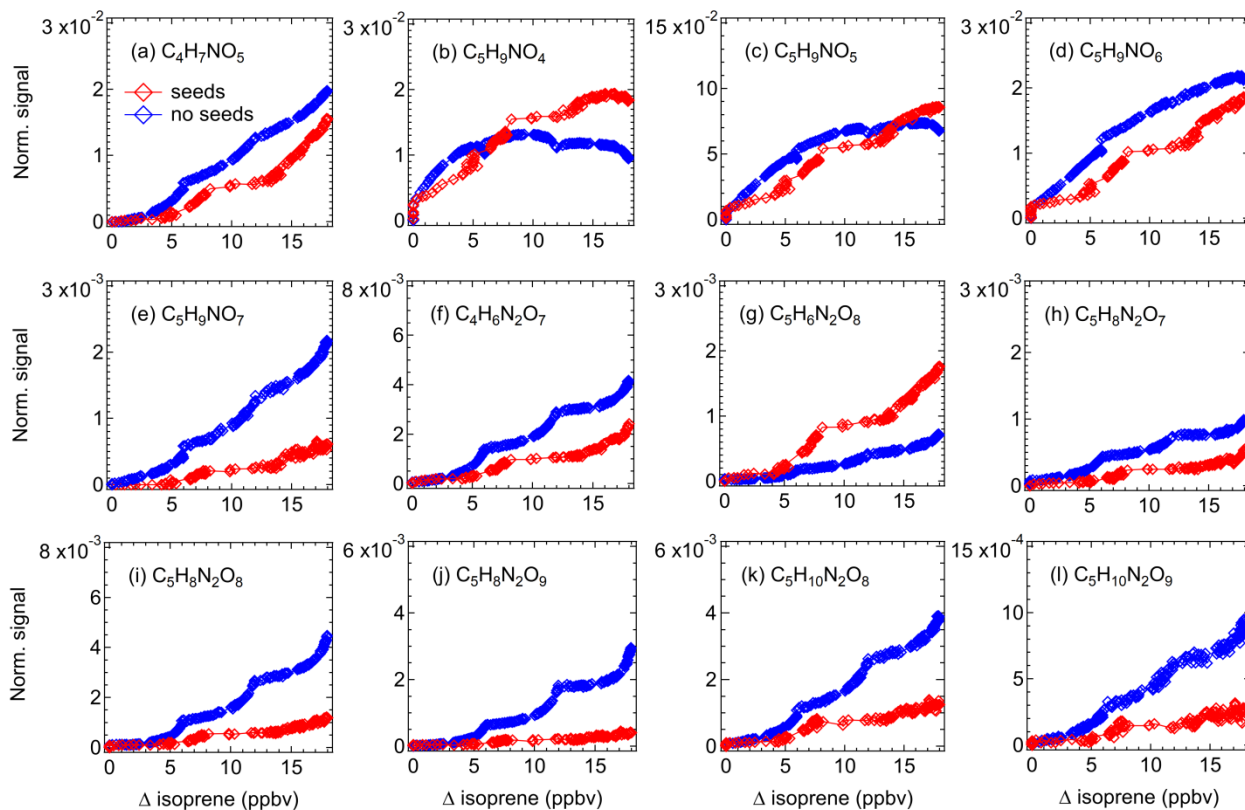
#### 795 3.3.1 C\* estimated by experimental methods

796 Detailed information about the volatility of organic molecules is essential to evaluate their potential to form  
797 SOA. In order to investigate the potential contribution of various isoprene oxidation products to SOA formation,  
798 we use our (limited) experimental data to estimate the vapor pressure of different isoprene organonitrates on the  
799 basis of their condensation behavior. Figure 6 shows how the signals of gas-phase products change in  
800 experiments with and without seed aerosols (ammonium sulfate). Please note that while the two experiments  
801 were conducted under similar conditions, the procedures could not be kept fully identical as aerosol seeding  
802 required specific measures and the oxidation chemistry might be slightly altered (e.g., due to initiation of  
803 heterogeneous reactions).

804 As shown in Fig. 6, the signals of most of the selected compounds decline when there are seed aerosols in  
805 the chamber, indicating that part of the condensable vapors is partitioned to the particle-phase due to the  
806 introduction of condensation sinks. The decrease in signal differs for different products, mostly depending on  
807 their vapor pressures. As expected, the lower volatility of a compound the higher the fraction that condenses.  
808 For instance, the signal of  $C_5H_9NO_7$  decreases by more than 70% in experiment with seed aerosols, compared to  
809 less than 40% on average for other less-oxidized 1N-monomers. In some cases (e.g.,  $C_5H_9NO_4$  and  $C_5H_9NO_5$ )  
810 however, the product signals in experiment with seed aerosols are higher than that without seeds after the  
811 consumed isoprene exceeding a certain level. In addition, the signal of  $C_5H_6N_2O_8$  in the experiment with seeds  
812 is always higher compared to that without seeds. One explanation for this phenomenon is the effect of  
813 heterogeneous reactions. It is likely that some condensed compound (denoted as A) can react on the particle  
814 surface to form new products with the molecular composition of compound B, or alternatively forming a  
815 precursor of B. When they evaporate back to the gas phase, it can result in an increase in signal of compound B.  
816 That's why a higher signal was observed for such compounds in experiment with seeds than that without seeds,  
817 as observed for  $C_5H_6N_2O_8$  in this case.

818 Based on the observed condensation behavior of different products, we can derive their vapor pressures  
819 from the gas-particle equilibrium partitioning coefficients by Eq. (2). As depicted in Fig. 7, the saturation  
820 concentrations of different organonitrates show a decreasing tendency from 1N-, 2N-monomer and 3N-  
821 monomers to 2N- and 3N-dimers, suggesting that dimers have a higher propensity of condensation and  
822 contribute to SOA formation. This is partly related to their molecular weight, as larger molecules generally have  
823 lower vapor pressures. However, it cannot explain all the features of the volatility distribution. For example,  
824  $C_5H_9NO_6$  (corresponding to No.8 in Fig.7) has higher mass than  $C_5H_9NO_5$  (corresponding to No.7 in Fig.7) but  
825 is predicted to have higher vapor pressure. In general, chemical composition and functionalities have significant  
826 effects on vapor pressure. For instance, the 2D-VBS composition-activity relationship suggests that each carbon  
827 and oxygen decrease  $C^*$  by 0.475 and 1.75 decades, respectively (Donahue et al., 2011). Different functional  
828 groups also have very different effect on volatility. For example, each hydroxyl group ( $-OH$ ) or hydroperoxy  
829 group ( $-OOH$ ) typically reduces the volatility by 2.4 to 2.5 decades, while the less polar carbonyl group ( $=O$ )  
830 reduces the volatility by 1 decade (Pankow and Asher 2008, Donahue et al., 2011). The nitrooxy group ( $-ONO_2$ )  
831 has a similar reductive effect on vapor pressure, which typically reduces  $C^*$  by 2.5 orders of magnitude (Pankow  
832 and Asher, 2008). Here, the irregularly high vapor pressure of  $C_5H_9NO_6$  is most likely attributed to the  
833 functional groups it contains. As listed in Table S2,  $C_5H_9NO_6$  is proposed to be nitrooxy hydroxy hydroperoxyl

834 compound, which consists of two highly polar functional groups –OH and –OOH, contributing to formation of  
 835 intramolecular H-bonding that can significantly increase the vapor pressure (Bilde et al., 2015; Kurten et al.,  
 836 2016), while  $C_5H_9NO_5$  only contains a –OOH group and hence cannot form intramolecular H-bonding. This  
 837 explanation is also valid for  $C_5H_9N_3O_{10}$  and  $C_5H_9N_3O_{12}$ . In summary, ~~These~~ findings underline that the  
 838 constitutional and configurational information of a molecule is critical for vapor-pressure estimation.



839  
 840 **Figure 6: Time evolution of selected major gas-phase products during experiments with (red) and without (blue) seed**  
 841 **aerosols (ammonium sulfate). Signals have been corrected for dilution.**

### 842 3.3.2 $C^*$ estimated by different parametrization methods

843 For comparison, we also adopt different parameterization methods to estimate the saturation vapor pressures of  
 844 isoprene oxidation products based on their molecular composition and the proposed structures, with the results  
 845 depicted in Fig. 7. In general, the saturation concentrations calculated by different parameterization methods  
 846 show a similar volatility distribution to that calculated by experimental method, with  $C^*$  of 1N-, 2N- and 3N-  
 847 monomers, 2N- and 3N-dimers decreasing in turn. However, different parameterization methods lead to the  
 848 predicted vapor concentrations with a variability of several orders of magnitude for the same compound, and the  
 849 discrepancies become larger and larger with more complicated molecules. In addition,  $C^*$  of structural isomers  
 850 calculated by the same method could span several decades.

851 As shown in Fig. 7, the Donahue et al. parameterization mostly provides lower  $C^*$  compared to the three  
 852 GC methods, with a maximum discrepancy up to 12 orders of magnitude for dimers. With regard to smaller and  
 853 less oxidized 1N-monomers, predicted  $C^*$  values from different methods are in relatively good agreement with  
 854 each other, whereas the disagreement increases to 11 orders of magnitude for 2N- and 3N-monomers. This is  
 855 mainly the case because the organic molecules were regarded as a mixture of =O and –OH functional groups in  
 856 the Donahue et al. parameterization, and their relative abundance was assumed to be 1:1 (Donahue et al., 2011).

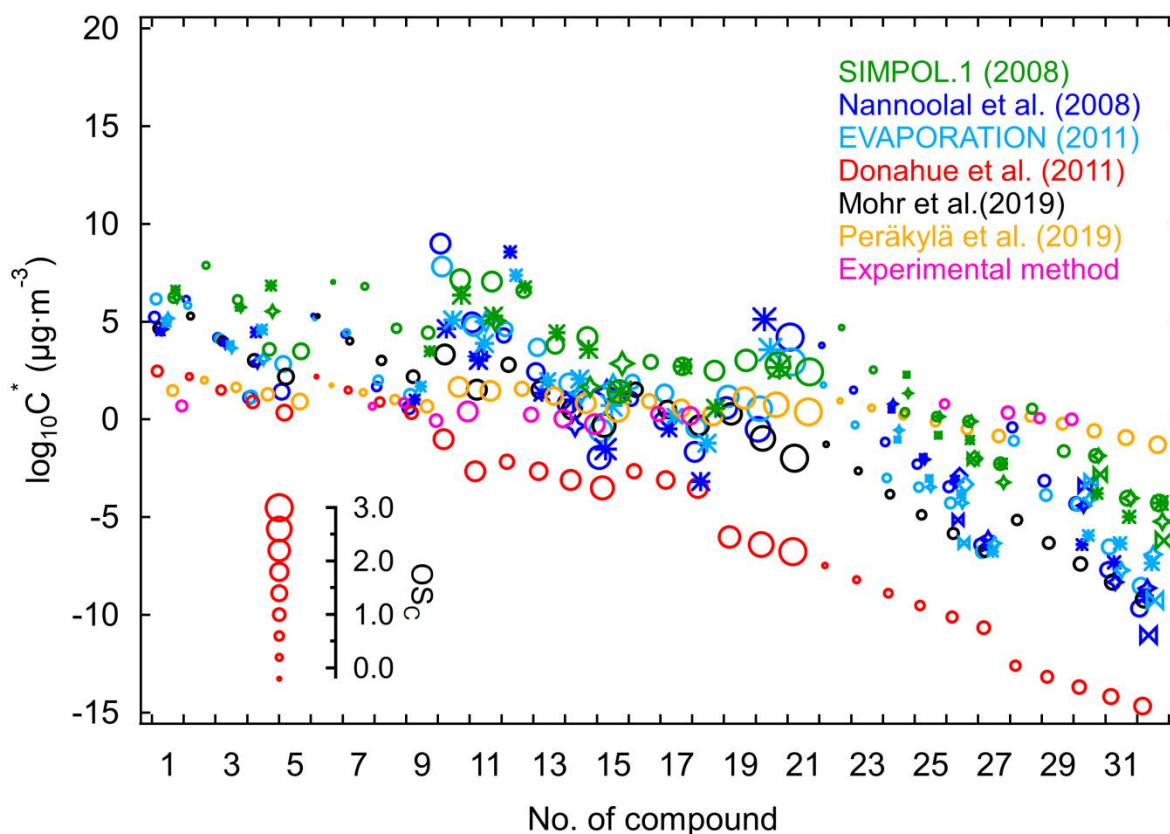
857 In consequence, the –OOH functional group in peroxides is treated as two –OH groups when adapting the  
858 method proposed by Donahue et al. (2011). However, it is demonstrated that the extra oxygen in peroxy  
859 moieties has little contribution to reduce vapor pressure (Pankow and Asher et al., 2008), hence treating –OOH  
860 equivalent to two –OH functional groups would underestimate the vapor pressures of hydroperoxyl compounds.  
861 Furthermore, organic compounds consisting of multiple polar functional groups (such as hydroperoxy, peroxy  
862 acid, and peroxide functional groups) tend to form intramolecular H-bonding, which would increase the vapor  
863 pressure (Bilde et al., 2015; Kurten et al., 2016). All these issues contribute to an underestimation of the vapor  
864 pressures of multifunctional products when using the Donahue et al. parameterization. Mohr et al. (2019)  
865 improved the parameterization for vapor-pressure estimation by taking the presence of –OOH functional groups  
866 in HOM explicitly into consideration and revising the parameters to reduce the effect of –OOH on depressing  $C^*$ .  
867 Consequently, the Mohr et al. parameterization effectively reduces the discrepancy between its estimates and  
868 those predicted by the GC methods, with the differences within 6 orders of magnitude. Nevertheless, there is a  
869 slight tendency to underestimate the vapor pressures of 3N-monomers and dimers. The Peräkylä et al.  
870 parameterization method, which was derived from measurements of the condensation behavior of HOM  
871 produced from  $\alpha$ -pinene ozonolysis, predicts similar  $C^*$  to Donahue et al. method for 1N-monomers, but higher  
872  $C^*$  for 2N- and 3N-monomers like the Mohr et al. method. As for dimers, especially for the 3N-dimers  
873 containing more multifunctional groups, the Peräkylä et al. method even predicts higher  $C^*$  than the GC  
874 methods in most cases.

875 Three GC methods predict similar saturation vapor pressures for different isoprene nitrates in this work,  
876 with the differences within 5 orders of magnitudes. Generally, the SIMPOL.1 method always provides higher  $C^*$   
877 compared to another two methods, and the disagreement between methods becomes larger for molecules  
878 containing multifunctional groups. For instance, the vapor-pressure discrepancy between SIMPOL.1 and  
879 another two GC methods are both 2 orders of magnitude for  $C_5H_9NO_{4,5}$  and  $C_{10}H_{17}N_3O_{12-14}$ , but it increased up  
880 to 4 and 5 orders of magnitude, respectively, for  $C_5H_9NO_{6,7}$  and  $C_{10}H_{17}N_3O_{15,16}$ .

881 It is worth noting that the Nannoolal et al. method is able to distinguish between positional isomers (e.g.,  
882 the estimated  $C^*$  for two  $C_5H_{10}N_2O_9$  isomers are 0.858 and 0.333  $\mu\text{g m}^{-3}$ , respectively), whereas such capacity of  
883 EVAPORATION method is limited (e.g., it is able to distinguish between the position isomers of  $C_5H_{10}N_2O_9$ ,  
884 but it predicts identical  $C^*$  for  $C_{10}H_{16}N_2O_{11}$  isomers). In this respect, the SIMPOL.1 method cannot distinguish  
885 between positional isomers at all. Moreover, SIMPOL.1 method predicts smaller differences between functional  
886 group isomers for 1N-monomers and 3N-dimers compared to the Nannoolal et al. method and the  
887 EVAPORATION, but there is no such regular pattern for 2N-monomers and 2N-dimers.

888 By comparing the results calculated by experimental method with those by different parameterization  
889 methods, we can see that the GC methods predict ~~lower-high~~ saturation concentrations for 1N-monomers than  
890 the experimental method, while the Donahue et al. and Peräkylä et al. method provide similar  $C^*$  values. With  
891 regard to 2N-monomers, the GC methods predict higher vapor pressures compared to the experimental method,  
892 ~~and-but~~ the discrepancy decreases with decreasing saturation concentration. The disagreement of  $C^*$  for 2N-  
893 monomers estimated by experimental method and the Mohr et al. or Peräkylä et al. method are within 2 orders  
894 of magnitude. In terms of low-volatility dimers, however, the vapor pressures calculated by the experimental  
895 method were 1–3 orders of magnitude larger than that predicted by the parameterization methods except for the  
896 Peräkylä et al. method. The Peräkylä et al. method provides the most similar predictions to the experimental

897 method for isoprene oxidation products in the full volatility range, with the disagreement within 1 order of  
898 magnitude.



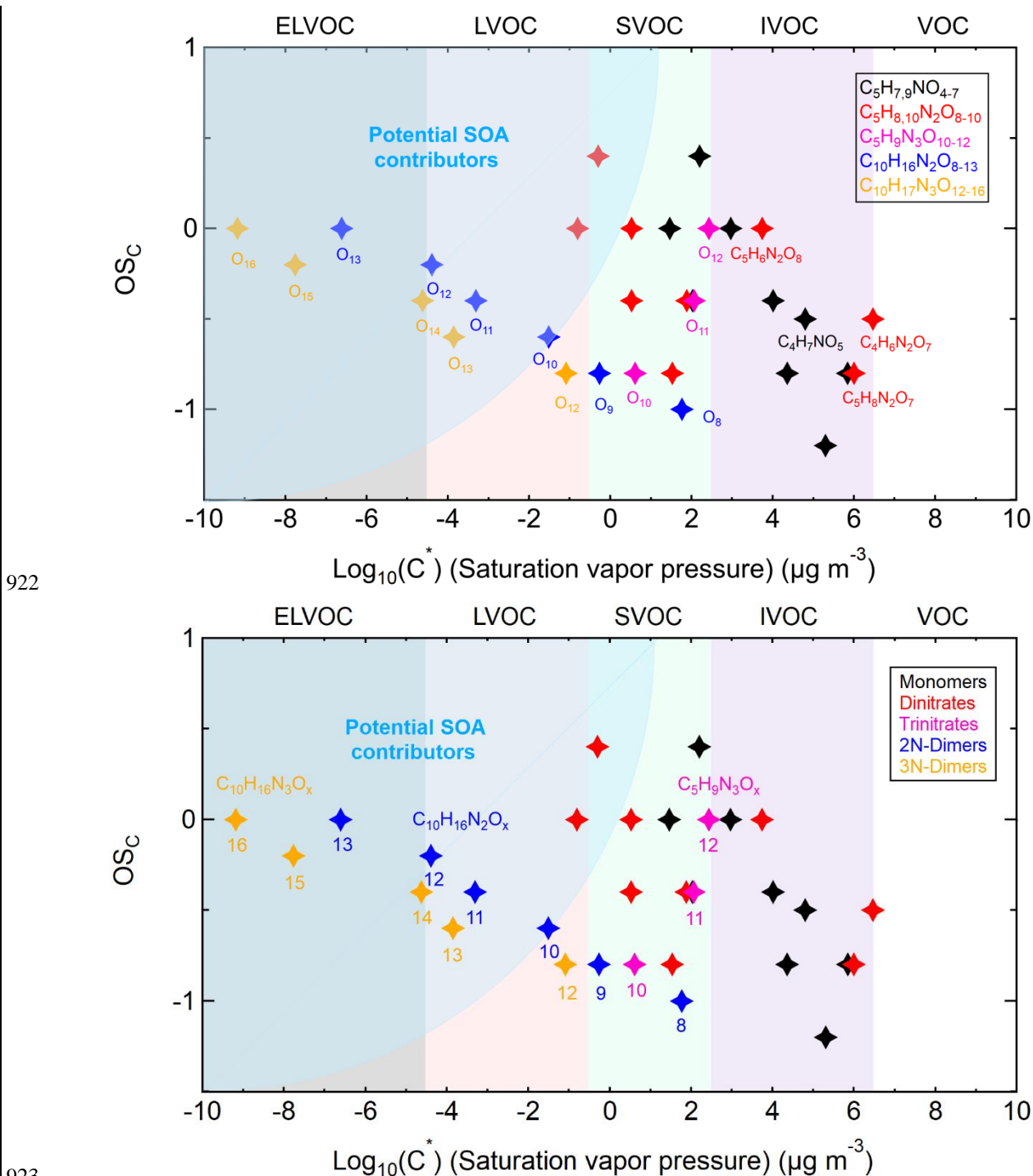
899  
900 **Figure 7: Saturation concentrations (in  $\mu\text{g m}^{-3}$ , at 298.15 K) of isoprene organonitrates estimated by using**  
901 **experimental and parameterization methods. The numbers correspond with the compound numbers of given in Table**  
902 **S2 (No. 1–9, 10–18, 19–21, 22–27, and 28–32 corresponding to 1N-monomers, 2N-monomers, 3N-monomer, 2N-**  
903 **dimers and 3N-dimers, respectively). Marker shapes indicate different isomers, with their size scaled by carbon**  
904 **oxidation state (*OSC*).**

905 In general, the vapor pressures estimated experimentally in this study are very close to that calculated by  
906 Peräkylä et al. method for which the estimation parameters were also derived experimentally. The discrepancy  
907 between the experimental and the GC methods spans several orders of magnitude depending on different  
908 compounds, with the GC methods predicting lower–higher  $C^*$  for less-functionalized 1N-monomers,  
909 approximate  $C^*$  for 2N-monomers, but higher–lower  $C^*$  for highly functionalized dimers. It is difficult to tell  
910 which method is more reliable without any measured saturation vapor pressure data on such multifunctional  
911 organic nitrates. However, considering the fact that the existing GC methods tend to underestimate saturation  
912 vapor pressures of the highly functionalized organic molecules due to their limited capability to deal with  
913 intramolecular interactions (e.g. the intramolecular hydrogen bonding formed among polar functional groups),  
914 and the well consistent results of two experimentally derived methods, we suggest that the experimental method  
915 might be a good choice to determine the volatility of highly oxidized compounds accurately.

### 916 3.3.3 Volatility distribution of isoprene nitrates and expected SOA yields.

917 Although the vapor pressures calculated by different methods show a variability of several orders of magnitude,  
918 the predicted volatility distributions of different organic groups are consistent. To eliminate the discrepancy  
919 caused by methods and get an average trend of the volatility distribution of various isoprene nitrates, we use the

920 median value of  $C^*$  calculated by different methods as the estimator of the vapor pressure for each nitrate  
 921 compound.



924 **Figure 8: Volatility distribution of different organonitrates formed from  $\text{NO}_3$ -initiated isoprene oxidation. The**  
 925 **volatility classes are indicated along the top with corresponding colors in the plot. The position of potential SOA**  
 926 **contributors is determined depending on the exact functionalities of molecules adapted from Bianchi et al. (2019).**

927 The average carbon oxidation state is plotted against  $\text{Log}_{10}(C^*)$  in Fig. 8 to describe the volatility  
 928 distribution of organic nitrates formed from isoprene oxidation by  $\text{NO}_3$ . Generally, the volatility of measured  
 929 gas-phase products spans a wide range from IVOC to ELVOC, wherein all of the 1N-monomers fall in the  
 930 IVOC or SVOC range, suggesting that 1N-monomers have low potential to form SOA by simple condensation

931 as long as the organic aerosol load is less than  $200 \mu\text{g m}^{-3}$ . The addition of a second or third  $-\text{NO}_3$  functional  
932 group decreases  $C^*$  of most 2N- and 3N-monomers by 2-3 decades compared with 1N-monomers, and most of  
933 them belong to SVOC. They will start to condense in significant fractions if the organic aerosol load is in a  
934 range of  $1\text{-}10 \mu\text{g m}^{-3}$ , which means 2N- and 3N-monomers with  $\text{OS}_c > -0.8$  may contribute to SOA formation  
935 under atmospheric conditions. With regard to dimers, all 3N-dimers and 2N-dimers (except for  $\text{C}_{10}\text{H}_{16}\text{N}_2\text{O}_{8,9}$ )  
936 are in LVOC or even ELVOC range, indicating isoprene dimers had high propensity to form SOA even at  
937 organic aerosol loads  $\ll 1 \mu\text{g/m}^3$ . However, we would like to emphasize here that the signals of 2N- and 3N-  
938 dimers only account for less than 2% on average of the total assigned signals, as shown in Fig. [S5S6](#). This  
939 suggests that the SOA yield of isoprene from  $\text{NO}_3$  oxidation by condensation should be low under atmospheric  
940 conditions.

941 The fate of  $\text{RO}_2$  determines the product distribution directly and hence could substantially affect SOA  
942 yields and aerosol physicochemical properties (Boyd et al., 2015; Fry et al., 2018; Ng et al., 2008; Schwantes et  
943 al., 2015; Ziemann and Atkinson, 2012). Consequently, it would be helpful to provide SOA yields together with  
944 the fate of  $\text{RO}_2$ . In our experiment, reactions with  $\text{HO}_2$  and  $\text{NO}_3$  the dominant loss channels for the initially  
945 formed  $\text{RO}_2$  from isoprene oxidation by  $\text{NO}_3$ , contributing for  $\sim 53\%$  and  $\sim 30\%$  of overall  $\text{RO}_2$  loss;  $\text{RO}_2 + \text{RO}_2$   
946 reactions contributed a minor fraction ( $\sim 13\%$ ) followed by unimolecular reactions with a contribution of  $\sim 5\%$ ,  
947 according to modelling results (Brownwood et al., 2021). More details about the modelling and the results can  
948 be found elsewhere (Brownwood et al., 2021; Vereecken et al., 2021).

949 In polluted urban regions, the fate of  $\text{RO}_2$  is typically dominated by  $\text{RO}_2 + \text{NO}_3$ , while in the more pristine  
950 environment, the  $\text{RO}_2 + \text{HO}_2$  reaction will dominate  $\text{RO}_2$  fate (Bianchi et al., 2019; Boyd et al., 2015; Brown  
951 and Stutz, 2012).  $\text{RO}_2 + \text{HO}_2$  was more important in the chamber than that in ambient and enhanced  $\text{RO}_2 + \text{HO}_2$   
952 would potentially lead to less dimer formation by  $\text{RO}_2 + \text{RO}_2$  reactions and hence reducing SOA yields.  
953 However, a recent work from Brownwood et al. (2021) based on the same campaign as this study pointed out  
954 that the bulk aerosol composition and SOA yields were largely independent of  $\text{RO}_2$  fate. Similarly, Boyd et al.  
955 (2015) found for  $\beta$ -pinene- $\text{NO}_3$  system that  $\text{RO}_2$  fate (“ $\text{RO}_2 + \text{NO}_3$  dominant” vs “ $\text{RO}_2 + \text{HO}_2$  dominant”) had  
956 only few effects on SOA formation. Therefore, the SOA yield estimated in this study is expected to be  
957 comparable to that in the atmosphere.

958 Assuming that the dimers in the LVOC or ELVOC range will condense onto particles, we estimated a SOA  
959 mass yield for condensation of isoprene organic nitrates of about  $5\% \pm 2\%$ . This value is based on an averaged  
960 bulk organonitrate sensitivity of  $0.019 \text{ norm. count s}^{-1} \text{ ppbv}^{-1}$  and has been corrected for wall loss and dilution  
961 (see Fig. [S6S7](#), with uncorrected SOA mass yield of about  $2\%$ ). The estimated SOA mass yield is within the  
962 range of those reported in the literature, but at the lower end ( $4.3\%$  to  $23.8\%$  depending on  $\text{RO}_2$  fate, Ng et al.,  
963 2008;  $0.7\%$  for first generation oxidation and  $14\%$  after oxidation of both double bonds, Rollins et al., 2009;  $27\%$   
964 on average for ambient measurements, Fry et al., 2018). The SOA yield will probably become somewhat higher  
965 if taking the contribution of ~~the minor dimer products as well as~~ SVOCs (including  $\text{C}_{10}\text{H}_{16}\text{N}_2\text{O}_8$ ,  $\text{C}_{10}\text{H}_{16}\text{N}_2\text{O}_9$   
966 and some other monomers, as shown in Fig. 8) into consideration. Our finding is commensurable with the SOA  
967 yield for isoprene organic nitrates of  $2\text{-}6\%$  derived from HR-AMS measurements in the same campaign  
968 (Brownwood et al., ~~in preparation~~2021).

969 In addition,  $\text{Br}^-$  adduct ionization CIMS is selective for  $\text{HO}_2$  and less oxidized organic compounds  
970 (Albrecht et al., 2019; Rissanen et al., 2019), so it is reasonable to assume that there were more highly oxidized

971 products that were not detected by Br<sup>-</sup> CIMS. This assumption is confirmed by measurements with a NO<sub>3</sub><sup>-</sup> CIMS  
972 performed in another isoprene-NO<sub>3</sub> experiment in SAPHIR (Zhao et al., ~~in preparation~~2021). Zhao et al. (2021)  
973 observed a higher fraction of dimers and more highly oxidized monomers and dimers, as well as trimers (C<sub>15</sub>  
974 compounds). As a consequence, the SOA yields derived from NO<sub>3</sub><sup>-</sup> CIMS measurements is slightly higher.

975 From these points of view our yield is more a lower limit. However, even if we assume an error of a factor  
976 of 2, the SOA yield of isoprene organic nitrates by condensation is more likely in a range of about 10% or less  
977 than in the higher range of 20-30% published in the literature. Of course, by our method we cannot cover any  
978 liquid phase processes that would lead to additional SOA beyond the condensation of the target compounds.

#### 979 4. Conclusions and implication

980 In this work, a gas-phase experiment conducted in the SAPHIR chamber under near atmospheric conditions in  
981 the dark was analyzed to primarily investigate the multi-generation chemistry of isoprene-NO<sub>3</sub> system. The  
982 characteristics of a diversity of isoprene nitrates were measured by the CIMS using Br<sup>-</sup> as the reagent ion.  
983 Isoprene 1N-, 2N-, and 3N-monomers and 2N- and 3N-dimers have different time behaviors, indicating the  
984 occurrence of multi-generation oxidation during this process. Based on their specific time behaviors as well as  
985 the general knowledge of isoprene and radical chemistry, the possible formation mechanisms of these  
986 compounds are proposed.

987 In order to evaluate the potential contribution of various isoprene nitrates to SOA formation, different  
988 composition-activity and group-contribution methods were used to estimate their saturation vapor pressures. We  
989 also calculated the vapor pressures of isoprene oxidation products based on the gas-particle equilibrium  
990 coefficients derived from condensation measurements. The vapor pressures estimated by different methods  
991 spans several orders of magnitude, and the discrepancies increase as the compounds become highly  
992 functionalized. It shows that existing composition-activity methods (especially the Donahue et al. method)  
993 seriously group-contribution methods tend to underestimate the saturation vapor pressure of the multifunctional  
994 low-volatility molecules compared to the experimental methods; The group-contribution methods seem to have  
995 a better performance than the CA methods on this aspect, but they still have a tendency to underestimate the  
996 vapor pressures of multifunctional molecules. ~~and we~~We suggest that experimental methods ~~might be~~is a good  
997 choice to estimate the volatility of highly oxidized compounds accurately.

998 According to our results, 1N-monomers and most 2N and 3N-nitrates fall in the IVOC or SVOC range.  
999 Therefore, they have, with a few exceptions, low potential to form SOA at atmospheric organic aerosol loads. In  
1000 contrast, 2N- and 3N-dimers are estimated to have low or extremely low volatility, indicating that they are  
1001 significant contributors to SOA formation, although dimers constitute less than 2% of the total explained signals.  
1002 In this study, no new particle formation events were observed. Assuming that the dimers in the LVOC or  
1003 ELVOC range will condense onto particles completely, we estimate a SOA mass yield of about 5 % ± 2 %,  
1004 which is a lower limit if one takes a possible contribution of the minor dimer products as well as SVOC species  
1005 into consideration. Both the volatility distribution and calculated SOA yields indicate that isoprene dimers  
1006 formed from NO<sub>3</sub> oxidation are the major contributors to SOA formation.



1007 **Data availability**

1008 All data given in figures can be displayed in tables or in digital form. This includes the data given in the  
1009 Supplement. Please send all requests for data to [t.mentel@fz-juelich.de](mailto:t.mentel@fz-juelich.de) and [r.wu@fz-juelich.de](mailto:r.wu@fz-juelich.de).

1010 **Author contributions**

1011 HF, JNC, JLF, SSB, AW, and AKS designed the study. Instrument deployment and data analysis were carried  
1012 out by RW, ET, SK, SRA, LH, AN, HF, RT, TH, PTMC, JS, FB, BB, JAT. RW, LV, ET, DZ, JAT, MH, TFM  
1013 interpreted the compiled data set. RW, TFM, LV wrote the manuscript. All co-authors discussed the results and  
1014 commented on the manuscript.

1015 **Competing interests**

1016 The authors declare that they have no conflict of interest.

1017 **Acknowledgements**

1018 This work has received funding from the European Research Council (ERC) and European Commission (EC)  
1019 under the European Union's Horizon 2020 research and innovation program (SARLEP grant agreement No.  
1020 681529, and Eurochamp 2020 grant agreement No. 730997 [and FORCeS, grant #No.-821205](#)). R.Wu gratefully  
1021 acknowledges the fellowship from Helmholtz-OCPC (Office of China Postdoc Council) Postdoc Program for  
1022 research support. [M. Hallquist, E. Tsiligiannis and Th. F. Mentel acknowledge support by the Swedish Research](#)  
1023 [Council \(grant numbers 2014-05332 and 2018-04430\) and FORMAS \(grant numbers 942-2015-1537 and xxx-](#)  
1024 [2020-yyyy\).](#)

1025 **References**

- 1026 Albrecht, S. R., Novelli, A., Hofzumahaus, A., Kang, S., Baker, Y., Mentel, T., Wahner, A., and Fuchs, H.:  
1027 Measurements of hydroperoxy radicals (HO<sub>2</sub>) at atmospheric concentrations using bromide chemical  
1028 ionisation mass spectrometry, *Atmos. Meas. Tech.*, 12, 891-902, 10.5194/amt-12-891-2019, 2019.
- 1029 Anglada, J. M., Crehuet, R., and Francisco, J. S.: The Stability of  $\alpha$ -Hydroperoxyalkyl Radicals, *Chem. Eur. J.*,  
1030 22, 18092-18100, 2016.
- 1031 Atkinson, R., and Arey, J.: Gas-phase tropospheric chemistry of biogenic volatile organic compounds: a review,  
1032 *Atmos. Environ.*, 37, 197-219, 10.1016/S1352-2310(03)00391-1, 2003.
- 1033 Atkinson, R.: Gas-phase tropospheric chemistry of organic compounds: a review, *Atmos. Environ.*, 41, 200-240,  
1034 10.1016/j.atmosenv.2007.10.068, 2007.
- 1035 Barber, V. P., Pandit, S., Green, A. M., Trongsirivat, N., Walsh, P. J., Klippenstein, S. J., and Lester, M. I.:  
1036 Four-carbon Criegee intermediate from isoprene ozonolysis: Methyl vinyl ketone oxide synthesis, infrared  
1037 spectrum, and OH production, *J. Am. Chem. Soc.*, 140, 10866-10880, 2018.
- 1038 Berndt, T., Mentler, B., Scholz, W., Fischer, L., Herrmann, H., Kulmala, M., and Hansel, A.: Accretion Product  
1039 Formation from Ozonolysis and OH Radical Reaction of alpha-Pinene: Mechanistic Insight and the

1040 Influence of Isoprene and Ethylene, *Environ. Sci. Technol.*, 52, 11069-11077, 10.1021/acs.est.8b02210,  
1041 2018.

1042 Bianchi, F., Kurten, T., Riva, M., Mohr, C., Rissanen, M. P., Roldin, P., Berndt, T., Crouse, J. D., Wennberg, P.  
1043 O., Mentel, T. F., Wildt, J., Junninen, H., Jokinen, T., Kulmala, M., Worsnop, D. R., Thornton, J. A.,  
1044 Donahue, N., Kjaergaard, H. G., and Ehn, M.: Highly Oxygenated Organic Molecules (HOM) from Gas-  
1045 Phase Autoxidation Involving Peroxy Radicals: A Key Contributor to Atmospheric Aerosol, *Chem. Rev.*,  
1046 119, 3472-3509, 10.1021/acs.chemrev.8b00395, 2019.

1047 Bilde, M., Barsanti, K., Booth, M., Cappa, C. D., Donahue, N. M., Emanuelsson, E. U., McFiggans, G., Krieger,  
1048 U. K., Marcolli, C., Topping, D., Ziemann, P., Barley, M., Clegg, S., Dennis-Smith, B., Hallquist, M.,  
1049 Hallquist, A. M., Khlystov, A., Kulmala, M., Mogensen, D., Percival, C. J., Pope, F., Reid, J. P., Ribeiro da  
1050 Silva, M. A., Rosenoern, T., Salo, K., Soonsin, V. P., Yli-Juuti, T., Prisle, N. L., Pagels, J., Rarey, J.,  
1051 Zardini, A. A., and Riipinen, I.: Saturation vapor pressures and transition enthalpies of low-volatility  
1052 organic molecules of atmospheric relevance: from dicarboxylic acids to complex mixtures, *Chem. Rev.*,  
1053 115, 4115-4156, 10.1021/cr5005502, 2015.

1054 Brown, S., Degouw, J., Warneke, C., Ryerson, T., Dubé, W., Atlas, E., Weber, R., Peltier, R., Neuman, J., and  
1055 Roberts, J.: Nocturnal isoprene oxidation over the Northeast United States in summer and its impact on  
1056 reactive nitrogen partitioning and secondary organic aerosol, *Atmos. Chem. Phys.*, 9, 3027-3042,  
1057 10.5194/acp-9-3027-2009, 2009.

1058 [Brown, S. S., and Stutz, J.: Nighttime radical observations and chemistry, \*Chem. Soc. Rev.\*, 41, 6405-6447,](#)  
1059 [2012.](#)

1060 [Brownwood, B., Turdziladze, A., Hohaus, T., Wu, R., Mentel, T. F., Carlsson, P. T., Tsiligiannis, E., Hallquist,](#)  
1061 [M., Andres, S., and Hantschke, L.: Gas-particle partitioning and SOA yields of organonitrate products from](#)  
1062 [NO<sub>3</sub>-initiated oxidation of isoprene under varied chemical regimes, \*ACS Earth Space Chem.\*, 2021.](#)

1063 [Boyd, C., Sanchez, J., Xu, L., Eugene, A. J., Nah, T., Tuet, W., Guzman, M. I., and Ng, N.: Secondary organic](#)  
1064 [aerosol formation from the  \$\beta\$ -pinene+ NO<sub>3</sub> system: effect of humidity and peroxy radical fate, \*Atmos.\*  
1065 \[Chem. Phys.\]\(#\), 15, 7497-7522, 2015.](#)

1066 Carlton, A. G., Wiedinmyer, C., and Kroll, J. H.: A review of Secondary Organic Aerosol (SOA) formation  
1067 from isoprene, *Atmos. Chem. Phys.*, 9, 4987-5005, 10.5194/acp-9-4987-2009, 2009.

1068 Compernelle, S., Ceulemans, K., and Müller, J. F.: EVAPORATION: a new vapour pressure estimation  
1069 method for organic molecules including non-additivity and intramolecular interactions, *Atmos. Chem. Phys.*,  
1070 11, 9431-9450, 10.5194/acp-11-9431-2011, 2011.

1071 Crosson, E.: A cavity ring-down analyzer for measuring atmospheric levels of methane, carbon dioxide, and  
1072 water vapor, *Appl. Phys. B*, 92, 403-408, 10.1007/s00340-008-3135-y, 2008.

1073 Crouse, J. D., Nielsen, L. B., Jørgensen, S., Kjaergaard, H. G., and Wennberg, P. O.: Autoxidation of Organic  
1074 Compounds in the Atmosphere, *J. Phys. Chem. Lett.*, 4, 3513-3520, 10.1021/jz4019207, 2013.

1075 [Dommen, J., Hellen, H., Saurer, M., Jaeggi, M., Siegwolf, R., Metzger, A., Duplissy, J., Fierz, M., and](#)  
1076 [Baltensperger, U.: Determination of the aerosol yield of isoprene in the presence of an organic seed with](#)  
1077 [carbon isotope analysis, \*Environ. Sci. Technol.\*, 43, 6697-6702, 2009.](#)

1078 Donahue, N. M., Robinson, A. L., Stanier, C. O., and Pandis, S. N.: Coupled partitioning, dilution, and chemical  
1079 aging of semivolatile organics, *Environ. Sci. Technol.*, 40, 2635-2643, 10.1021/es052297c, 2006.

1080 Donahue, N. M., Epstein, S. A., Pandis, S. N., and Robinson, A. L.: A two-dimensional volatility basis set: 1.  
1081 organic-aerosol mixing thermodynamics, *Atmos. Chem. Phys.*, 11, 3303-3318, 10.5194/acp-11-3303-2011,  
1082 2011.

1083 Donahue, N. M., Kroll, J. H., Pandis, S. N., and Robinson, A. L.: A two-dimensional volatility basis set – Part 2:  
1084 Diagnostics of organic-aerosol evolution, *Atmos. Chem. Phys.*, 12, 615-634, 10.5194/acp-12-615-2012,  
1085 2012.

1086 Dubé, W. P., Brown, S. S., Osthoff, H. D., Nunley, M. R., Ciciora, S. J., Paris, M. W., McLaughlin, R. J., and  
1087 Ravishankara, A.: Aircraft instrument for simultaneous, in situ measurement of NO<sub>3</sub> and N<sub>2</sub>O<sub>5</sub> via  
1088 pulsed cavity ring-down spectroscopy, *Rev. Sci. Instrum.*, 77, 034101, 10.1063/1.2176058, 2006.

1089 Ehn, M., Thornton, J. A., Kleist, E., Sipila, M., Junninen, H., Pullinen, I., Springer, M., Rubach, F., Tillmann, R.,  
1090 Lee, B., Lopez-Hilfiker, F., Andres, S., Acir, I. H., Rissanen, M., Jokinen, T., Schobesberger, S.,  
1091 Kangasluoma, J., Kontkanen, J., Nieminen, T., Kurten, T., Nielsen, L. B., Jorgensen, S., Kjaergaard, H. G.,  
1092 Canagaratna, M., Maso, M. D., Berndt, T., Petaja, T., Wahner, A., Kerminen, V. M., Kulmala, M.,  
1093 Worsnop, D. R., Wildt, J., and Mentel, T. F.: A large source of low-volatility secondary organic aerosol,  
1094 *Nature*, 506, 476-479, 10.1038/nature13032, 2014.

1095 Friedman, B., and Farmer, D. K.: SOA and gas phase organic acid yields from the sequential photooxidation of  
1096 seven monoterpenes, *Atmos. Environ.*, 187, 335-345, 10.1016/j.atmosenv.2018.06.003, 2018.

1097 Fry, J. L., Brown, S. S., Middlebrook, A. M., Edwards, P. M., Campuzano-Jost, P., Day, D. A., Jimenez, J. L.,  
1098 Allen, H. M., Ryerson, T. B., Pollack, I., Graus, M., Warneke, C., de Gouw, J. A., Brock, C. A., Gilman, J.,  
1099 Lerner, B. M., Dubé, W. P., Liao, J., and Welti, A.: Secondary organic aerosol (SOA) yields from  
1100 NO<sub>3</sub> radical + isoprene based on nighttime aircraft power plant plume transects, *Atmos.*  
1101 *Chem. Phys.*, 18, 11663-11682, 10.5194/acp-18-11663-2018, 2018.

1102 Guenther, A., Jiang, X., Heald, C., Sakulyanontvittaya, T., Duhl, T., Emmons, L., and Wang, X.: The Model of  
1103 Emissions of Gases and Aerosols from Nature version 2.1 (MEGAN2. 1): an extended and updated  
1104 framework for modeling biogenic emissions, *Geosci. Model Dev.*, 5, 1471–1492, 10.5194/gmd-5-1471-  
1105 2012, 2012. .

1106 Hallquist, M., Wenger, J., Baltensperger, U., Rudich, Y., Simpson, D., Claeys, M., Dommen, J., Donahue, N.,  
1107 George, C., and Goldstein, A.: The formation, properties and impact of secondary organic aerosol: current  
1108 and emerging issues, *Atmos. Chem. Phys.*, 9, 5155–5236, 10.5194/acp-9-5155-2009, 2009 .

1109 Hu, J., Wu, L., Zheng, B., Zhang, Q., He, K., Chang, Q., Li, X., Yang, F., Ying, Q., and Zhang, H.: Source  
1110 contributions and regional transport of primary particulate matter in China, *Environ. Pollut.*, 207, 31-42,  
1111 10.1016/j.envpol.2015.08.037, 2015.

1112 [Jenkin, M. E., Valorso, R., Aumont, B., and Rickard, A. R.: Estimation of rate coefficients and branching ratios](#)  
1113 [for reactions of organic peroxy radicals for use in automated mechanism construction, \*Atmos. Chem. Phys.\*,](#)  
1114 [19, 7691–7717, <https://doi.org/10.5194/acp-19-7691-2019>, 2019.](#)

1115 Jenkin, M., Young, J., and Rickard, A.: The MCM v3. 3.1 degradation scheme for isoprene, *Atmos. Chem.*  
1116 *Phys.*, 15, 11433–11459, 10.5194/acp-15-11433-2015, 2015.

1117 Jimenez, J. L., Canagaratna, M., Donahue, N., Prevot, A., Zhang, Q., Kroll, J. H., DeCarlo, P. F., Allan, J. D.,  
1118 Coe, H., and Ng, N.: Evolution of organic aerosols in the atmosphere, *science*, 326, 1525-1529,  
1119 10.1126/science.1180353, 2009.

1120 Kim, P. S., Jacob, D. J., Fisher, J. A., Travis, K., Yu, K., Zhu, L., Yantosca, R. M., Sulprizio, M. P., Jimenez, J.  
1121 L., Campuzano-Jost, P., Froyd, K. D., Liao, J., Hair, J. W., Fenn, M. A., Butler, C. F., Wagner, N. L.,  
1122 Gordon, T. D., Welti, A., Wennberg, P. O., Crouse, J. D., St. Clair, J. M., Teng, A. P., Millet, D. B.,  
1123 Schwarz, J. P., Markovic, M. Z., and Perring, A. E.: Sources, seasonality, and trends of southeast US  
1124 aerosol: an integrated analysis of surface, aircraft, and satellite observations with the GEOS-Chem  
1125 chemical transport model, *Atmos. Chem. Phys.*, 15, 10411-10433, 10.5194/acp-15-10411-2015, 2015.

1126 Kirkby, J., Duplissy, J., Sengupta, K., Frege, C., Gordon, H., Williamson, C., Heinritzi, M., Simon, M., Yan, C.,  
1127 Almeida, J., Trostl, J., Nieminen, T., Ortega, I. K., Wagner, R., Adamov, A., Amorim, A., Bernhammer, A.  
1128 K., Bianchi, F., Breitenlechner, M., Brilke, S., Chen, X., Craven, J., Dias, A., Ehrhart, S., Flagan, R. C.,  
1129 Franchin, A., Fuchs, C., Guida, R., Hakala, J., Hoyle, C. R., Jokinen, T., Junninen, H., Kangasluoma, J.,  
1130 Kim, J., Krapf, M., Kurten, A., Laaksonen, A., Lehtipalo, K., Makhmutov, V., Mathot, S., Molteni, U.,  
1131 Onnela, A., Perakyla, O., Piel, F., Petaja, T., Praplan, A. P., Pringle, K., Rap, A., Richards, N. A., Riipinen,  
1132 I., Rissanen, M. P., Rondo, L., Sarnela, N., Schobesberger, S., Scott, C. E., Seinfeld, J. H., Sipila, M.,  
1133 Steiner, G., Stozhkov, Y., Stratmann, F., Tome, A., Virtanen, A., Vogel, A. L., Wagner, A. C., Wagner, P.  
1134 E., Weingartner, E., Wimmer, D., Winkler, P. M., Ye, P., Zhang, X., Hansel, A., Dommen, J., Donahue, N.  
1135 M., Worsnop, D. R., Baltensperger, U., Kulmala, M., Carslaw, K. S., and Curtius, J.: Ion-induced  
1136 nucleation of pure biogenic particles, *Nature*, 533, 521-526, 10.1038/nature17953, 2016.

1137 Kleindienst, T. E., Lewandowski, M., Offenberg, J. H., Jaoui, M., and Edney, E. O.: Ozone-isoprene reaction:  
1138 Re-examination of the formation of secondary organic aerosol, *Geophys. Res. Lett.*, 34,  
1139 10.1029/2006GL027485, 2007.

1140 Krechmer, J., Lopez-Hilfiker, F., Koss, A., Hutterli, M., Stoermer, C., Deming, B., Kimmel, J., Warneke, C.,  
1141 Holzinger, R., Jayne, J., Worsnop, D., Fuhrer, K., Gonin, M., and de Gouw, J.: Evaluation of a New  
1142 Reagent-Ion Source and Focusing Ion-Molecule Reactor for Use in Proton-Transfer-Reaction Mass  
1143 Spectrometry, *Anal. Chem.*, 90, 12011-12018, 10.1021/acs.analchem.8b02641, 2018.

1144 Kroll, J. H., Ng, N. L., Murphy, S. M., Flagan, R. C., and Seinfeld, J. H.: Secondary organic aerosol formation  
1145 from isoprene photooxidation, *Environ. Sci. Technol.*, 40, 1869-1877, 10.1021/es0524301, 2006.

1146 Kroll, J. H., Donahue, N. M., Jimenez, J. L., Kessler, S. H., Canagaratna, M. R., Wilson, K. R., Altieri, K. E.,  
1147 Mazzoleni, L. R., Wozniak, A. S., Bluhm, H., Mysak, E. R., Smith, J. D., Kolb, C. E., and Worsnop, D. R.:  
1148 Carbon oxidation state as a metric for describing the chemistry of atmospheric organic aerosol, *Nat. Chem.*,  
1149 3, 133-139, 10.1038/nchem.948, 2011.

1150 Kurten, T., Tiusanen, K., Roldin, P., Rissanen, M., Luy, J.-N., Boy, M., Ehn, M., and Donahue, N.:  $\alpha$ -Pinene  
1151 autoxidation products may not have extremely low saturation vapor pressures despite high O: C ratios, *J.*  
1152 *Phys. Chem. A*, 120, 2569-2582, 10.1021/acs.jpca.6b02196, 2016.

1153 Kwan, A., Chan, A., Ng, N., Kjærsgaard, H. G., Seinfeld, J., and Wennberg, P.: Peroxy radical chemistry and OH  
1154 radical production during the NO<sub>3</sub>-initiated oxidation of isoprene, *Atmos. Chem. Phys.*, 12, 7499-7515,  
1155 10.5194/acp-12-7499-2012, 2012.

1156 Marais, E. A., Jacob, D. J., Jimenez, J. L., Campuzano-Jost, P., Day, D. A., Hu, W., Krechmer, J., Zhu, L., Kim,  
1157 P. S., Miller, C. C., Fisher, J. A., Travis, K., Yu, K., Hanisco, T. F., Wolfe, G. M., Arkinson, H. L., Pye, H.  
1158 O. T., Froyd, K. D., Liao, J., and McNeill, V. F.: Aqueous-phase mechanism for secondary organic aerosol

1159 formation from isoprene: application to the southeast United States and co-benefit of SO<sub>2</sub> emission  
1160 controls, *Atmos. Chem. Phys.*, 16, 1603-1618, 10.5194/acp-16-1603-2016, 2016.

1161 McFiggans, G., Mentel, T. F., Wildt, J. r., Pullinen, I., Kang, S., Kleist, E., Schmitt, S., Springer, M., Tillmann,  
1162 R., Wu, C., Zhao, D., Hallquist, M., Faxon, C., Le Breton, M., Hallquist, A. s. M., Simpson, D., Bergström,  
1163 R., Jenkin, M. E., Ehn, M., Thornton, J. A., Alfarra, M. R., Bannan, T. J., Percival, C. J., Priestley, M.,  
1164 Topping, D., and Kiendler-Scharr, A.: Secondary organic aerosol reduced by mixture of atmospheric  
1165 vapours, *Nature*, 565, 587-593, 10.1038/s41586-018-0871-y, 2019.

1166 Mentel, T. F., Springer, M., Ehn, M., Kleist, E., Pullinen, I., Kurtén, T., Rissanen, M., Wahner, A., and Wildt, J.:  
1167 Formation of highly oxidized multifunctional compounds: autoxidation of peroxy radicals formed in the  
1168 ozonolysis of alkenes – deduced from structure–product relationships, *Atmos. Chem. Phys.*, 15, 6745-6765,  
1169 10.5194/acp-15-6745-2015, 2015.

1170 Mohr, C., Thornton, J. A., Heitto, A., Lopez-Hilfiker, F. D., Lutz, A., Riipinen, I., Hong, J., Donahue, N. M.,  
1171 Hallquist, M., Petaja, T., Kulmala, M., and Yli-Juuti, T.: Molecular identification of organic vapors driving  
1172 atmospheric nanoparticle growth, *Nat. Commun.*, 10, 4442, 10.1038/s41467-019-12473-2, 2019.

1173 Molteni, U., Simon, M., Heinritzi, M., Hoyle, C. R., Bernhammer, A.-K., Bianchi, F., Breitenlechner, M., Brilke,  
1174 S., Dias, A., Duplissy, J., Frege, C., Gordon, H., Heyn, C., Jokinen, T., Kürten, A., Lehtipalo, K.,  
1175 Makhmutov, V., Petäjä, T., Pieber, S. M., Praplan, A. P., Schobesberger, S., Steiner, G., Stozhkov, Y.,  
1176 Tomé, A., Tröstl, J., Wagner, A. C., Wagner, R., Williamson, C., Yan, C., Baltensperger, U., Curtius, J.,  
1177 Donahue, N. M., Hansel, A., Kirkby, J., Kulmala, M., Worsnop, D. R., and Dommen, J.: Formation of  
1178 Highly Oxygenated Organic Molecules from  $\alpha$ -Pinene Ozonolysis: Chemical Characteristics, Mechanism,  
1179 and Kinetic Model Development, *ACS Earth Space Chem.*, 3, 873-883,  
1180 10.1021/acsearthspacechem.9b00035, 2019.

1181 Mutzel, A., Rodigast, M., Iinuma, Y., Böge, O., and Herrmann, H.: Monoterpene SOA – Contribution of first-  
1182 generation oxidation products to formation and chemical composition, *Atmos. Environ.*, 130, 136-144,  
1183 10.1016/j.atmosenv.2015.10.080, 2016.

1184 Nannoolal, Y., Rarey, J., Ramjugernath, D., and Cordes, W.: Estimation of pure component properties: Part 1.  
1185 Estimation of the normal boiling point of non-electrolyte organic compounds via group contributions and  
1186 group interactions, *Fluid Phase Equilib.*, 226, 45-63, 10.1016/j.fluid.2004.09.001, 2004.

1187 Nannoolal, Y., Rarey, J., and Ramjugernath, D.: Estimation of pure component properties: Part 3. Estimation of  
1188 the vapor pressure of non-electrolyte organic compounds via group contributions and group interactions,  
1189 *Fluid Phase Equilib.*, 269, 117-133, 10.1016/j.fluid.2008.04.020, 2008.

1190 Ng, N., Kwan, A., Surratt, J., Chan, A., Chhabra, P., Sorooshian, A., Pye, H. O., Crounse, J., Wennberg, P., and  
1191 Flagan, R.: Secondary organic aerosol (SOA) formation from reaction of isoprene with nitrate radicals  
1192 (NO<sub>3</sub>), *Atmos. Chem. Phys.*, 8, 4117–4140, 10.5194/acp-8-4117-2008, 2008.

1193 Ng, N. L., Chhabra, P. S., Chan, A. W. H., Surratt, J. D., Kroll, J. H., Kwan, A. J., McCabe, D. C., Wennberg, P.  
1194 O., Sorooshian, A., Murphy, S. M., Dalleska, N. F., Flagan, R. C., and Seinfeld, J. H.: Effect of  
1195 NO<sub>x</sub> level on secondary organic aerosol (SOA) formation from the photooxidation of terpenes,  
1196 *Atmos. Chem. Phys.*, 7, 5159-5174, 10.5194/acp-7-5159-2007, 2007.

1197 Ng, N. L., Brown, S. S., Archibald, A. T., Atlas, E., Cohen, R. C., Crowley, J. N., Day, D. A., Donahue, N. M.,  
1198 Fry, J. L., Fuchs, H., Griffin, R. J., Guzman, M. I., Herrmann, H., Hodzic, A., Iinuma, Y., Jimenez, J. L.,

1199 Kiendler-Scharr, A., Lee, B. H., Luecken, D. J., Mao, J., McLaren, R., Mutzel, A., Osthoff, H. D., Ouyang,  
1200 B., Picquet-Varrault, B., Platt, U., Pye, H. O. T., Rudich, Y., Schwantes, R. H., Shiraiwa, M., Stutz, J.,  
1201 Thornton, J. A., Tilgner, A., Williams, B. J., and Zaveri, R. A.: Nitrate radicals and biogenic volatile  
1202 organic compounds: oxidation, mechanisms, and organic aerosol, *Atmos. Chem. Phys.*, 17, 2103-2162,  
1203 10.5194/acp-17-2103-2017, 2017.

1204 Novelli, A., Cho, C., Fuchs, H., Hofzumahaus, A., Rohrer, F., Tillmann, R., Kiendler-Scharr, A., Wahner, A.,  
1205 and Vereecken, L.: Experimental and theoretical study on the impact of a nitrate group on the chemistry of  
1206 alkoxy radicals, *Phys. Chem. Chem. Phys.*, 23, 5474–5495, <https://doi.org/10.1039/d0cp05555g>, 2021.

1207 Novelli, A., Vereecken, L., Bohn, B., Dorn, H.-P., Gkatzelis, G. I., Hofzumahaus, A., Holland, F., Reimer, D.,  
1208 Rohrer, F., and Rosanka, S.: Importance of isomerization reactions for OH radical regeneration from the  
1209 photo-oxidation of isoprene investigated in the atmospheric simulation chamber SAPHIR, *Atmos. Chem.*  
1210 *Phys.*, 20, 3333–3355, 10.5194/acp-20-3333-2020, 2020.

1211 O'Meara, S., Booth, A. M., Barley, M. H., Topping, D., and McFiggans, G.: An assessment of vapour pressure  
1212 estimation methods, *Phys. Chem. Chem. Phys.*, 16, 19453-19469, 10.1039/c4cp00857j, 2014.

1213 Orlando, J. J., Tyndall, G. S., and Wallington, T. J.: The atmospheric chemistry of alkoxy radicals, *Chem. Rev.*,  
1214 103, 4657-4690, 10.1021/cr020527p, 2003.

1215 Orlando, J. J., and Tyndall, G. S.: Laboratory studies of organic peroxy radical chemistry: an overview with  
1216 emphasis on recent issues of atmospheric significance, *Chem. Soc. Rev.*, 41, 6294-6317,  
1217 10.1039/C2CS35166H, 2012.

1218 Pankow, J. F., and Asher, W. E.: SIMPOL.1: a simple group contribution method for predicting vapor pressures  
1219 and enthalpies of vaporization of multifunctional organic compounds, *Atmos. Chem. Phys.*, 8, 2773-2796,  
1220 10.5194/acp-8-2773-2008, 2008.

1221 Peeters, J., Müller, J.-F. o., Stavrou, T., and Nguyen, V. S.: Hydroxyl radical recycling in isoprene oxidation  
1222 driven by hydrogen bonding and hydrogen tunneling: The upgraded LIM1 mechanism, *J. Phys. Chem. A*,  
1223 118, 8625-8643, 10.1021/jp5033146, 2014.

1224 Peräkylä, O., Riva, M., Heikkinen, L., Quéléver, L., Roldin, P., and Ehn, M.: Experimental investigation into the  
1225 volatilities of highly oxygenated organic molecules (HOM), *Atmos. Chem. Phys.*, 20, 649–669,  
1226 10.5194/acp-20-649-2020, 2020.

1227 Pöschl, U.: Atmospheric aerosols: composition, transformation, climate and health effects, *Angew. Chem. Int.*  
1228 *Ed.*, 44, 7520-7540, 10.1002/anie.200501122, 2005.

1229 Praske, E., Otkjær, R. V., Crouse, J. D., Hethcox, J. C., Stoltz, B. M., Kjaergaard, H. G., and Wennberg, P. O.:  
1230 Atmospheric autoxidation is increasingly important in urban and suburban North America, *Proc. Natl.*  
1231 *Acad. Sci. U.S.A.*, 115, 64-69, 10.1073/pnas.1715540115, 2018.

1232 Rissanen, M. P., Kurten, T., Sipila, M., Thornton, J. A., Kangasluoma, J., Sarnela, N., Junninen, H., Jorgensen,  
1233 S., Schallhart, S., Kajos, M. K., Taipale, R., Springer, M., Mentel, T. F., Ruuskanen, T., Petaja, T.,  
1234 Worsnop, D. R., Kjaergaard, H. G., and Ehn, M.: The formation of highly oxidized multifunctional  
1235 products in the ozonolysis of cyclohexene, *J. Am. Chem. Soc.*, 136, 15596-15606, 10.1021/ja507146s,  
1236 2014.

1237 Rissanen, M. P., Mikkilä, J., Iyer, S., and Hakala, J.: Multi-scheme chemical ionization inlet (MION) for fast  
1238 switching of reagent ion chemistry in atmospheric pressure chemical ionization mass spectrometry (CIMS)  
1239 applications, *Atmos. Meas. Tech.*, 12, 6635–6646, 10.5194/amt-12-6635-2019, 2019.

1240 Riva, M., Rantala, P., Krechmer, J. E., Peräkylä, O., Zhang, Y., Heikkinen, L., Garmash, O., Yan, C., Kulmala,  
1241 M., Worsnop, D., and Ehn, M.: Evaluating the performance of five different chemical ionization techniques  
1242 for detecting gaseous oxygenated organic species, *Atmos. Meas. Tech.*, 12, 2403-2421, 10.5194/amt-12-  
1243 2403-2019, 2019.

1244 Rohrer, F., Bohn, B., Brauers, T., Brüning, D., Johnen, F. J., Wahner, A., and Kleffmann, J.: Characterisation of  
1245 the photolytic HONO-source in the atmosphere simulation chamber SAPHIR, *Atmos. Chem. Phys.*, 5,  
1246 2189-2201, 10.5194/acp-5-2189-2005, 2005.

1247 Rollins, A. W., Kiendler-Scharr, A., Fry, J., Brauers, T., Brown, S. S., Dorn, H.-P., Dubé, W. P., Fuchs, H.,  
1248 Mensah, A., and Mentel, T.: Isoprene oxidation by nitrate radical: alkyl nitrate and secondary organic  
1249 aerosol yields, *Atmos. Chem. Phys.*, 9, 6685–6703, 10.5194/acp-9-6685-2009, 2009.

1250 Schwantes, R. H., Teng, A. P., Nguyen, T. B., Coggon, M. M., Crouse, J. D., St Clair, J. M., Zhang, X.,  
1251 Schilling, K. A., Seinfeld, J. H., and Wennberg, P. O.: Isoprene NO<sub>3</sub> Oxidation Products from the RO<sub>2</sub> +  
1252 HO<sub>2</sub> Pathway, *J. Phys. Chem. A*, 119, 10158-10171, 10.1021/acs.jpca.5b06355, 2015.

1253 Schwantes, R. H., Charan, S. M., Bates, K. H., Huang, Y., Nguyen, T. B., Mai, H., Kong, W., Flagan, R. C., and  
1254 Seinfeld, J. H.: Low-volatility compounds contribute significantly to isoprene secondary organic aerosol  
1255 (SOA) under high-NO<sub>x</sub> conditions, *Atmos. Chem. Phys.*, 19,  
1256 7255-7278, 10.5194/acp-19-7255-2019, 2019.

1257 Sobanski, N., Schuladen, J., Schuster, G., Lelieveld, J., and Crowley, J. N.: A five-channel cavity ring-down  
1258 spectrometer for the detection of NO<sub>2</sub>, NO<sub>3</sub>, N<sub>2</sub>O<sub>5</sub>, total peroxy nitrates and total alkyl nitrates, *Atmos.*  
1259 *Meas. Tech.*, 9, 5103–5118, 10.5194/amt-9-5103-2016, 2016.

1260 Spracklen, D., Jimenez, J., Carslaw, K., Worsnop, D., Evans, M., Mann, G., Zhang, Q., Canagaratna, M., Allan,  
1261 J., and Coe, H.: Aerosol mass spectrometer constraint on the global secondary organic aerosol budget,  
1262 *Atmos. Chem. Phys.*, 11, 12109–12136, 10.5194/acp-11-12109-2011, 2011.

1263 Stadler, S., Kühn, T., Schröder, S., Taraborrelli, D., Schultz, M. G., and Kokkola, H.: Isoprene-derived  
1264 secondary organic aerosol in the global aerosol–chemistry–climate model ECHAM6.3.0–HAM2.3–  
1265 MOZI.0, *Geosci. Model Dev.*, 11, 3235-3260, 10.5194/gmd-11-3235-2018, 2018.

1266 [Starn, T., Shepson, P., Bertman, S., Riemer, D., Zika, R., and Olszyna, K.: Nighttime isoprene chemistry at an](#)  
1267 [urban - impacted forest site, \*J. Geophys. Res. Atmos.\*, 103, 22437-22447, 1998.](#)

1268 [Stroud, C., Roberts, J., Williams, E., Hereid, D., Angevine, W., Fehsenfeld, F., Wisthaler, A., Hansel, A.,](#)  
1269 [Martinez - Harder, M., and Harder, H.: Nighttime isoprene trends at an urban forested site during the 1999](#)  
1270 [Southern Oxidant Study, \*J. Geophys. Res. Atmos.\*, 107, ACH 7-1-ACH 7-14, 2002.](#)

1271 Suh, I., Lei, W., and Zhang, R.: Experimental and Theoretical Studies of Isoprene Reaction with NO<sub>3</sub>, *J. Phys.*  
1272 *Chem. A*, 105, 6471-6478, 10.1021/jp0105950, 2001.

1273 Surratt, J. D., Chan, A. W., Eddingsaas, N. C., Chan, M., Loza, C. L., Kwan, A. J., Hersey, S. P., Flagan, R. C.,  
1274 Wennberg, P. O., and Seinfeld, J. H.: Reactive intermediates revealed in secondary organic aerosol  
1275 formation from isoprene, *Proc. Natl. Acad. Sci. U.S.A.*, 107, 6640-6645, 10.1073/pnas.0911114107, 2010.

1276 Thornton, J. A., Shilling, J. E., Shrivastava, M., D'Ambro, E. L., Zawadowicz, M. A., and Liu, J.: A Near-  
1277 Explicit Mechanistic Evaluation of Isoprene Photochemical Secondary Organic Aerosol Formation and  
1278 Evolution: Simulations of Multiple Chamber Experiments with and without Added NO<sub>x</sub>, *ACS Earth Space*  
1279 *Chem.*, 10.1021/acsearthspacechem.0c00118, 2020.

1280 Tröstl, J., Chuang, W. K., Gordon, H., Heinritzi, M., Yan, C., Molteni, U., Ahlm, L., Frege, C., Bianchi, F., and  
1281 Wagner, R.: The role of low-volatility organic compounds in initial particle growth in the atmosphere,  
1282 *Nature*, 533, 527-531, 10.1038/nature18271, 2016.

1283 Vereecken, L., Nguyen, T. L., Hermans, I., and Peeters, J.: Computational study of the stability of  $\alpha$ -  
1284 hydroperoxyl-or  $\alpha$ -alkylperoxyl substituted alkyl radicals, *Chem. Phys. Lett.*, 393, 432-436,  
1285 10.1016/j.cplett.2004.06.076, 2004.

1286 Vereecken, L.: Computational study of the stability of  $\alpha$ -nitroxy-substituted alkyl radicals, *Chem. Phys. Lett.*,  
1287 466, 127-130, 10.1016/j.cplett.2008.10.042, 2008.

1288 Vereecken, L., and Peeters, J.: Decomposition of substituted alkoxy radicals—part I: a generalized structure–  
1289 activity relationship for reaction barrier heights, *Phys. Chem. Chem. Phys.*, 11, 9062-9074,  
1290 10.1039/B909712K, 2009.

1291 Vereecken, L., and Peeters, J.: A structure–activity relationship for the rate coefficient of H-migration in  
1292 substituted alkoxy radicals, *Phys. Chem. Chem. Phys.*, 12, 12608-12620, 10.1039/C0CP00387E, 2010.

1293 Vereecken, L., and Francisco, J. S.: Theoretical studies of atmospheric reaction mechanisms in the troposphere,  
1294 *Chem. Soc. Rev.*, 41, 6259-6293, 10.1039/C2CS35070J, 2012.

1295 Vereecken, L., and Nozière, B.: H migration in peroxy radicals under atmospheric conditions, *Atmos. Chem.*  
1296 *Phys.*, 20, 7429-7458, 10.5194/acp-20-7429-2020, 2020.

1297 [Vereecken, L., Carlsson, P., Novelli, A., Bernard, F., Brown, S. S., Cho, C., Crowley, J. N., Fuchs, H., Mellouki,](#)  
1298 [W., Reimer, D., Shenolikar, Justin, Tillmann, R., Zhou, L., Kiendler-Scharr, A., and Wahner, A.:](#)  
1299 [Theoretical and experimental study of peroxy and alkoxy radicals in the NO<sub>3</sub>-initiated oxidation of](#)  
1300 [isoprene, \*Phys. Chem. Chem. Phys.\*, 23, 5496–5515, <https://doi.org/10.1039/d0cp06267g>, 2021.](#)

1301 Wang, S., Riva, M., Yan, C., Ehn, M., and Wang, L.: Primary formation of highly oxidized multifunctional  
1302 products in the OH-Initiated oxidation of Isoprene: a combined theoretical and experimental study, *Environ.*  
1303 *Sci. Technol.*, 52, 12255-12264, 10.1021/acs.est.8b02783, 2018.

1304 [Warneke, C., De Gouw, J., Goldan, P., Kuster, W., Williams, E., Lerner, B., Jakoubek, R., Brown, S., Stark, H.,](#)  
1305 [and Aldener, M.: Comparison of daytime and nighttime oxidation of biogenic and anthropogenic VOCs](#)  
1306 [along the New England coast in summer during New England Air Quality Study 2002, \*J. Geophys. Res.\*](#)  
1307 [Atmos., 109, 2004.](#)

1308 Wennberg, P. O., Bates, K. H., Crouse, J. D., Dodson, L. G., McVay, R. C., Mertens, L. A., Nguyen, T. B.,  
1309 Praske, E., Schwantes, R. H., and Smarte, M. D.: Gas-phase reactions of isoprene and its major oxidation  
1310 products, *Chem. Rev.*, 118, 3337-3390, 10.1021/acs.chemrev.7b00439, 2018.

1311 Whalley, L., Stone, D., and Heard, D.: New insights into the tropospheric oxidation of isoprene: combining field  
1312 measurements, laboratory studies, chemical modelling and quantum theory, in: *Atmospheric and Aerosol*  
1313 *Chemistry*, edited by: McNeill, V. F., and Ariya, P. A., Springer, Berlin, Heidelberg, Germany, 55-95,  
1314 10.1007/128\_2012\_359, 2012.

1315 Zhang, Q., Jimenez, J. L., Canagaratna, M., Allan, J., Coe, H., Ulbrich, I., Alfarra, M., Takami, A., Middlebrook,  
1316 A., and Sun, Y.: Ubiquity and dominance of oxygenated species in organic aerosols in anthropogenically -  
1317 influenced Northern Hemisphere midlatitudes, *Geophys. Res. Lett.*, 34, 10.1029/2007GL029979, 2007.



1318 [Zhao, D., Pullinen, I., Fuchs, H., Schrade, S., Wu, R., Acir, I.-H., Tillmann, R., Rohrer, F., Wildt, J., and Guo,](#)  
1319 [Y.: Highly oxygenated organic molecules \(HOM\) formation in the isoprene oxidation by NO<sub>3</sub> radical,](#)  
1320 [Atmos. Chem. Phys. Discuss., 1-28, 2020.](#)  
1321 Ziemann, P. J., and Atkinson, R.: Kinetics, products, and mechanisms of secondary organic aerosol formation,  
1322 Chem. Soc. Rev., 41, 6582-6605, 10.1039/c2cs35122f, 2012.